DEVELOPMENT OF COPPER PHYLLOSILICATE CATALYSTS FOR CATALYTIC TRANSFER HYDROGENATION OF FURFURAL TO HIGH VALUE PRODUCTS

MISS TANYARAT SHOOSRI

A THESIS SUBMITTED IN PARTIAL FULFILLMENT OF THE
REQUIREMENT FOR THE DEGREE OF MASTER IN APPILED CHEMISTRY
DEPARTMENT OF CHEMISTRY SCHOOL OF SCIENCE
KING MONGKUT'S INSTITUTE OF TECHNOLOGY LADKRABANG
2022

KMITL-2022-SC-M-012-124

Thesis Title	Development of copper phyllosilicate catalysts for catalytic transfer hydrogenation of furfural to high value products
Student	Miss Tanyarat Shoosri
Student ID	63605042
Degree	Master of Science (Applied Chemistry)
Department	Chemistry
Year	2022
Thesis Advisor	Asst. Prof. Dr. Patcharaporn Weerachawanasak
Thesis Coadvisor	Prof. Dr. Tawan Sooknoi, Dr. Sanchai Kuboon

Abstract

The study on the conversion of furfural to GVL over CuPS in liquid phase catalytic transfer hydrogenation have been investigated. In this work divided in three parts. The catalysts studied including i) copper loading and copper species, ii) physical mixing, and iii) secondary metal. For the copper loading and copper species, it was found 30%CuPS-R shows the complete furfural conversion while, 30%CuPS shows high GVL selectivity. It can be noted that the metallic Cu^0 species on reduced CuPS catalyst act as active species for hydrogenation of furfural to furfuryl alcohol while CuO species on calcined CuPS catalyst play an important role to convert furfuryl alcohol to GVL. Therefore, the physical mixing between 30%CuPS-R and 30%CuPS have been studied with various ratio. For physical mixing ratio (50:50), the GVL was reached to 86% with complete furfural conversion (100%). The conversion and selectivity were improved by the synergistic between metallic Cu^0 species and Cu^{2+} species. For the secondary metal (Mn_2O_3 and ZnO) were prepared by incipient wetness impregnation method. It was found the 1%Mn_2O_3/CuPS and 1%ZnO/CuPS gave the selective hydrogenation of furfural to furfuryl alcohol.

Keyword: hydrogenation, furfural, furfuryl alcohol, phyllosilicate, γ-valerolactone

ACKNOWLEDGEMENT

The authors take this opportunity to acknowledge advisors Assst. Prof. Dr. Patcharaporn Weerachawanasak and Co-Advisor Prof. Dr. Tawan Sooknoi and Dr. Sanchai Kuboon, for the continually suggestion, graceful knowledge, and useful discussion throughout this research. In addition, we would like to sincere appreciate chairperson and committee member, Prof. Dr. Joongjai Panpranot and Asst. Prof. Dr. Chaval Sriwong, respectively, for the opinions and the guidance with a graceful.

Financial supports from the Thailand Graduate Institute of Science and Technology: TGIST scholarship for Miss Tanyarat Shoosri (Grant number: SCA-CO-2563-12176-TH) from the national science and technology development agency are gratefully acknowledged.

We would like to distribute a kindness thank to Catalytic Chemistry Research Unit members for their contribution of the ideas and facilities and most importantly their support. We would like to extend our thanks to Mr. Bunyarat Rungtaweevoranit and Miss Sutarat Thongratkaew for their help and advice in working the characterization at National Nanotechnology Center (NANOTEC), support and encouragement.

Furthermore, we would like to express our appreciation thanks to Department of Chemistry, Faculty of Science, King Mongkut's Institute of Technology Ladkrabang for advanced laboratory instruments, equipment, chemical and accommodation.

Last but not least, the authors would like to gracefully thank the parents and families, who give an encouragement. This thesis would not be possible without them. The thesis is dedicated for the world citizen, who want to be a technical and theoretical expert.

Tanyarat Shoosri

CONTENTS

CONTENTS (CONTINUED)

Page

CONTENTS (CONTINUED)

Page

LIST OF TABLES

Table **Page**

.

LIST OF FIGURES

Figure **Page**

CHAPTER 1
INTRODUCTION

1.1 INTRODUCTION

The demands of fossil fuel resources, such as petroleum, coal, natural gas, etc. have been dramatically increased as the main precursors for production of energy and chemicals. Since the limit of fossil fuels resources and the serious emission of CO_2 gas that would not be friendly to the environment, an alternative energy is critical to solving these problems because it is environmentally friendly and sustainable. Lignocellulose biomass has been interesting because the main compositions consisted of cellulose, hemicellulose, and lignin that are low-price sustainable carbon sources. [1][2]. Therefore, they can be the supplier to produce the biomass-derived platform chemicals. One of them, Furfural is a key chemical intermediate which receives from the acid-catalyzed hydrolysis and dehydration of hemicellulose. The conversion of furfural to various high value products have been performed via a variety of reactions such as decarboxylation, oxidation, decarbonylation, and hydrogenation. Among of these, hydrogenation was widely used to produce many desired products such as furfuryl alcohol (FA), tetrahydrofurfuryl alcohol (THFA), levulinic acid (LA), furfuryl alkyl ethers (FEs), or γ - valerolactone (GVL)[3][4]. However, GVL is one of the versatile chemicals that extensively used in a variety of applications, including green solvent in fine chemical synthesis, biopolymer building block, flavoring agent, illuminating liquid, fuel additive, and lighter fluid[5]

In general, GVL production utilizes high molecular H_2 pressure resulting in high production costs, particularly in the large scale. Alternative process for reducing the production costs such as catalytic transfer hydrogenation via the Meerwein-Ponndorf-Verley (MPV) reaction using hydrogen donor has recently been developed. **Figure 1.1**

shows the overall reaction pathway of furfural to GVL. Furfural was first transformed to furfuryl alcohol (FA) utilizing alcohol as an H-donor via the MPV reaction, and then furfuryl ether (FE) was formed by etherified. Then, FE transformed by hydrolytic ring-opening to isopropyl levulinate (IPL) by using Brønsted acids as a catalyst.

Furthermore, FE can be transformed to - or β-angelica lactone (- or -AL), which can then be hydrolyzed and etherified to create IPL. Finally, using Lewis' acids as a catalyst, IPL undergoes an MPV reaction and subsequent lactonization to create GVL. Recently, The development of efficient and cost-effective reaction pathways for the conversion of furfural to GVL has emerged as an interesting issue in biomass energy use research. According to the reaction pathways for furfural hydrogenation to GVL, both type of acids, (Lewis and Brønsted acid) is strongly influenced to control the possible direction of furfural transformations to GVL. The noble and non-noble metal catalysts such as Au/ZrO_2- ZSM-5, Zr-Al-beta-zeolite, Sn-Al-beta zeolite, Zr-HY, Al-HY, etc. have been reported to be active in this reaction because they contained the suitable. Lewis and Brønsted acid sites[6–8]. That However, synthesis of a suitable composition between the Lewis and Brønsted acid sites is very challenging. Moreover, non-noble metal catalysts for direct synthesis of GVL from furfural has not much reported. Therefore, the design and development of non-noble metal catalyst for direct synthesis of GVL from furfural via MPV reaction is very attractive.

In this work, copper phyllosilicate (CuPS) structure has an interesting catalyst because it has both of Lewis and Brønsted acid properties in the structure. The copper phyllosilicate structure consists of unsaturated coordinative Cu ions in the octahedral layer acting as the Lewis acid sites and the OH groups on the surface acting as the Brønsted acid sites [9]. Furthermore, the phyllosilicate structure could provide highly metal dispersion when catalyst has high metal loading. However, the suitable amount of copper loading in phyllosilicate structure for direct conversion of furfural to GVL has never bee

studied and reported. Beside the highly dispersion, the acid properties of copper phyllosilicate could be tuning by controlling the amount of metal/metal oxide species on the catalyst. Therefore, the effect of metallic Cu°/CuO on copper phyllosilicate catalysts have been comparatively studied. Moreover, adding of second metal such as Mn_2O_3, ZnO on the copper phyllosilicate have also studied. Finally, the characteristic and catalytic behavior of copper phyllosilicate catalysts should be evaluated.

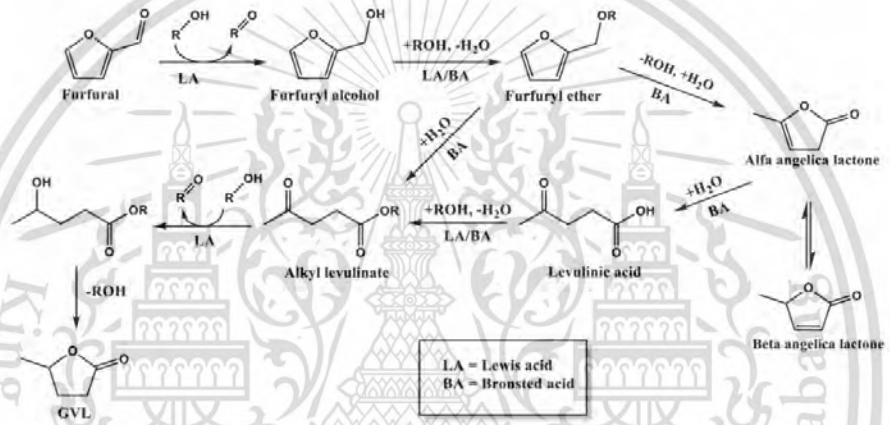

Figure 1.1. Reaction pathway of direct conversion of furfural to GVL [6]

1.2 Objectives of the study

1. 2. 1 To design and develop copper phyllosilicate catalysts for the catalytic transfer hydrogenation of furfural to GVL.

1. 2. 2 To study the effect of copper loading, the metallic Cu^0/CuO species on copper phyllosilicate catalysts in the catalytic transfer hydrogenation of furfural to GVL.

1. 2. 3 To study the effect of secondary metal loading such as ZnO, Mn_2O_3 on copper phyllosilicate catalysts for the catalytic transfer hydrogenation of furfural to GVL.

1.2.4 To investigate the characteristics and catalytic properties of copper phyllosilicate catalysts for the catalytic transfer hydrogenation of furfural to GVL.

1.3 Scopes of the study

1.3.1 The copper phyllosilicate catalysts with various amount of copper loading (10-30 % wt.) will be prepared by ammonia evaporation hydrothermal method.

1.3.2 The reduced and calcined copper phyllosilicate catalysts will be comparatively studied in catalytic transfer hydrogenation of furfural to GVL.

1.3.3 The secondary metals loading such as ZnO and Mn_2O_3, will be added on suitable copper phyllosilicate catalyst by incipient wetness impregnation method.

1.3.4 All catalysts will be characterized by the following techniques.

- X-ray diffraction (XRD)
- X-ray fluorescence spectroscopy (XRF)
- N_2-physisorption (BET)
- H_2 temperature-programmed reduction (H_2-TPR)
- NH_3 temperature programmed desorption (NH_3-TPD)
- X-ray photoelectron spectroscopy (XPS)
- Pyridine adsorption FTIR spectra (Py-IR)

1.3.5 The catalysts will be investigated the catalytic performance in liquid phase hydrogenation of furfural to GVL.

1.4 Benefits of the study

1.4.1 To obtain the highly efficiency catalysts for the liquid phase hydrogenation of furfural to GVL via CTH reaction.

1.4.2 To understand the reaction pathways of catalytic transfer hydrogenation of furfural to GVL by using copper phyllosilicate catalysts.

1.4.3 To tuning the acid properties of copper phyllosilicate catalyst for the direct conversion of furfural to GVL.

CHAPTER 2

THEORY AND LITERATURE REVIEWS

2.1 Furfural

Furfural is a green bio-based chemical produced from lignocellulose. It can be produced from sugar dehydration, which occurs in a variety of agricultural byproducts such as corncobs, oats, wheat bran, and sawdust. Typically, furfural appears as an oily colorless liquid which has an almond-like odor. The color of furfural can turn from yellow to dark brown when it longer presents in air. The physical properties of furfural are summarized in **Table 2.1**.[5]

Table 2.1 Physical properties of furfural

Properties	**Values**
Molecular formula	$C_5H_4O_2$
Structure	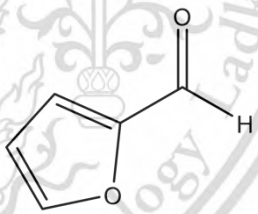
Molecular weight ($gmol^{-1}$)	96.1
Boiling point (°C)	161.7
Melting point	-37
Density at 20 °C (g/ml)	1.16
Solubility in water (g/L)	83
Vapor pressure (mmHg, 20°C)	2

Furfural is heteroaromatic furan ring with an aldehyde functional group, resulting in furfural is an attractive platform molecule because it may be used as a chemical substrate to produce fuels, solvents, and high-value compounds. Furfural can undergo various reactions and provide a range of useful compound such as acylation, acetylation, reductive amination to amines, decarboxylation, oxidation to carboxylic acids, Grignard reactions and aldol and Knoevenagel condensation can occur in furfural through the aldehyde functional group. The reactions like alkylation, hydrogenation, oxidation, halogenation, open ring reactions, and nitration are enabled through the furan-ring system. The possible catalytic reactions of furfural to various products are illustrated in **Figure 2.1.** [5][10]. Among of these reaction, hydrogenation of furfural route is a versatility reaction because it could directly produce gamma-valerolactone (GVL), which is useful chemical and expensive fuel.

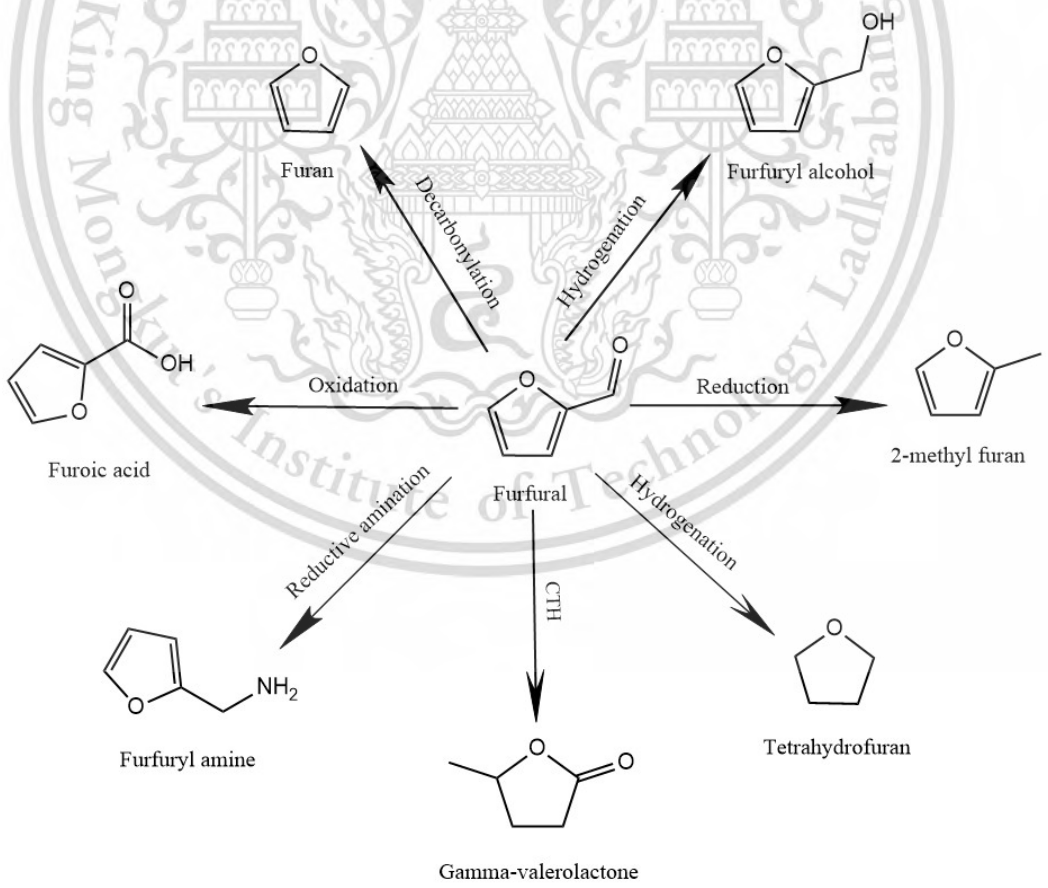

Figure 2.1 The possible catalytic reactions of furfural to various products.

Recent advances in the hydrogenation of furfural to furan derivatives have primarily focused on catalytic processes utilizing various types of metal based catalysts, such as non-noble metal (Cu, Ni, Co, etc.)[11–13] and noble metal (Pd, Pt, Ru, etc.) [14,15]under hydrogen pressure (carried out in the presence of molecular H_2), which is a high-pressure condition

2.2 Gamma-Valerolactone (GVL)

GVL has good solvent abilities and is a precursor for high-value chemicals and fuels. A traditionally GVL can be produced by hydrogenation Levulinic acid and ester GVL is a colorless liquid that is stable under normal conditions and has a sweet. GVL is liquid at normal conditions and has a high boiling point. The physical properties of GVL are summarized in **table 2.2.** [4]. GVL can be used for platform chemical such as fuel additive, jet fuels or diesel fuels and green solvent

Table 2.2 Physical properties of GVL

Properties	**Values**
Molecular formula	$C_5H_8O_2$
Structure	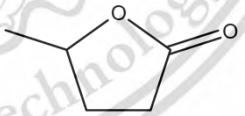
Molecular weight ($gmol^{-1}$)	100.116
Boiling point (°C)	205
Melting point	-31
Density at 20 °C (g/ml)	1.0546
Solubility in water (mg/ml)	≥100

The possibilities application as shown in **Figure 2.2** are based on two deoxygenated compounds formed from GVL: pentenoic acid and valeric acid. Pentenoic acid can be deoxygenated further by decarboxylation and oligomerized to a combination of C8+ alkanes similar to jet fuels. Valeric acid also has two concurrent processes: esterification to alkyl esters (biodiesel) and deoxygenation and oligomerisation via 5-nonanone to C9 alkanes/olefins (diesel/gasoline fuels).

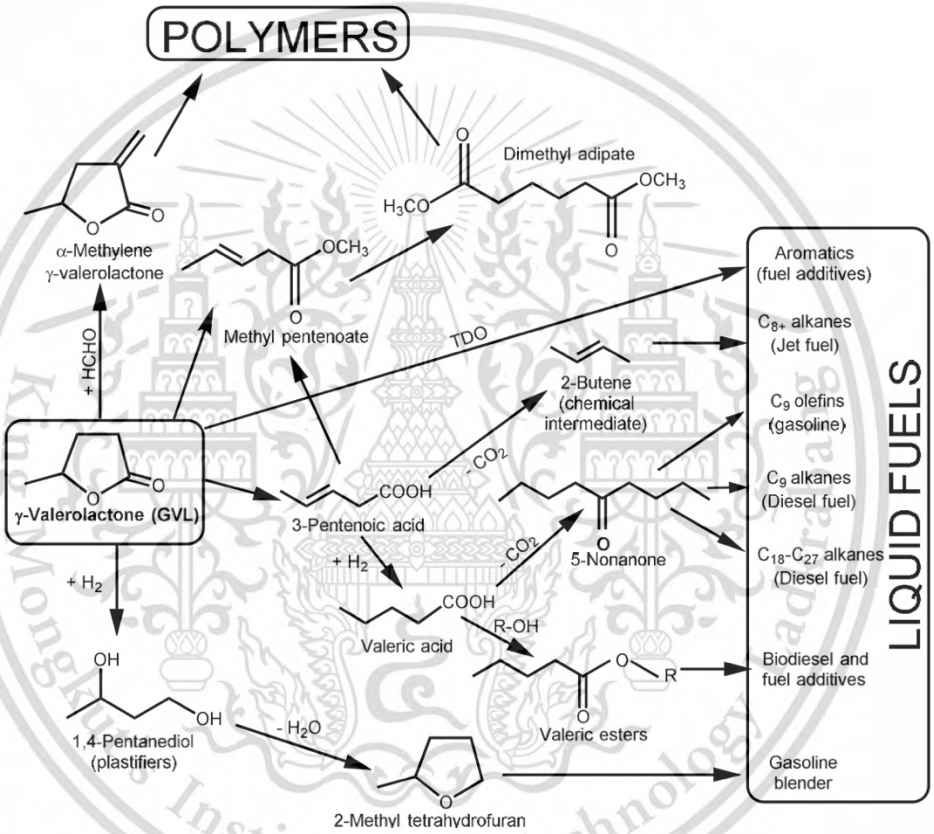

Figure 2.2 the production of fuels and chemicals from GVL [4].

2.3 Meerwein–Ponndorf–Verley reduction (MPV)

The MPV reaction involves the transfer of hydrogen from an alcohol (usually a secondary alcohol) to a carbonyl group and effective method for synthesizing carbonyl compounds under very mild conditions. The process has been extensively studied in heterogeneous catalyst. The widely used are metal oxide include acid, basic properties.

For MPV reduction of furfural, the reaction occurs on Lewis's acid sites of catalyst, which is reported that can promote hydrogen transfer from secondary alcohols to carbonyl groups through a six-membered ring intermediate. The hydrogenation via the Meerwein-Ponndorf - Verley (MPV) reduction where secondary alcohol serves as the hydrogen donor, has intensively attention because it is environmentally friendly, safe, easy, and low-cost operation[16,17].

2.4 Direct synthesis of biomass-derived furfural to GVL

GVL is generally formed by hydrogenating levulinic acid (LA) and its esters[18]. The hydrogenation process may be utilized to convert LA to GVL in two ways: catalytic transfer hydrogenation using formic acid or an alcohol as the hydrogen donor or high-pressure hydrogenation with external hydrogen[19][20]. Furfuryl alcohol and furfural may also produce GVL. The direct conversion of furfural to GVL, in particular, is still under investigation. As a result, developing efficient and cost-effective reaction pathways for the conversion of furfural into GVL has emerged as an interesting issue in the field of biomass energy utilization research. A catalyst containing both Lewis and Bronsted catalysts is required for the reaction.

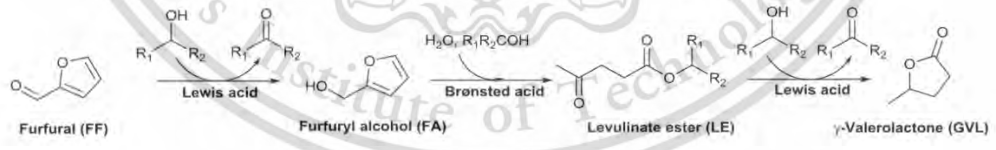

Figure 2.3 shows the direct synthesis of GVL from furfural.

The conventional process of the conversion of FAL to GVL is composed of many reaction steps as shown in **Figure 2.3** exhibits the transformation of furfural (FF) to furfuryl alcohol (FA), followed by rearrangement to levulinate ester (LE). The levulinate ester might then be hydrogenated by lactonization to generate GVL. Typically, the hydrogenation in

the first and third steps may be accomplished by employing gaseous H_2 at high pressures, resulting in a high-cost operation and lack of safety. One of the alternate ways, hydrogenation via the Meerwein-Ponndorf-Verley (MPV) reduction[21].

Furfuryl alcohol (FA) to furfuryl ether(FE) conversion requires the Lewis acid site and the Brønsted acid site . FE is then transformed to alkyl levulinate (isopropyl levulinate, IPL) by hydrolytic ring-opening processes catalyzed by Brnsted acids. Furthermore, FE can be changed to - or -angelica lactone - or -AL) and then to alkyl levulinate. Finally, when utilizing a Lewis acid catalyst, alkyl levulinate undergoes an MPV reaction and subsequent lactonization to create GVL, as shown in **Figure 2.4.** It can be concluded that, lewis acid site as well as Brønsted acid site of catalyst, are needed for the transformation of furfural (FF) to GVL[6].

From the aforementioned, both Lewis as well as Brønsted acid catalysts are required in a catalyst. The suitable catalyst is required to proceed the reaction. It is known to be that catalyst occupied the Lewis acid site is needed to initiate and proceed the hydrogen transfer from secondary alcohol to substances.

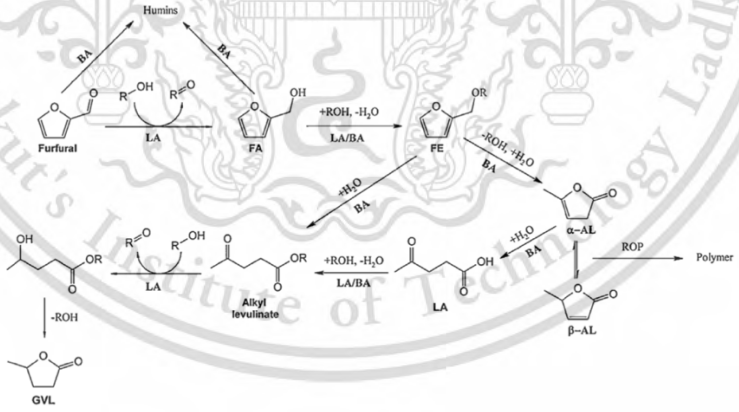

Figure 2.4 Reaction pathway for the conversion of furfural to GVL [6].

2.5 Phyllosilicate

The basic structure of the phyllosilicates is based on repeating unit of interconnected six-membered rings of SiO_4^{4-} tetrahedral sheet and second metal octahedral in infinite dimensions. In the tetrahedral sheet, three oxygen atoms possessed in each tetrahedral unit forming the hexagon with OH^- anion at the center[22]. This leads to a basic structural unit of $Si_2O_5(OH)^{3-}$. While an assemble in octahedral layer composed of metal cation center, usually Ni^{2+}, Cu^{2+} or others. The oxygen in octahedral layer would coordinate with the oxygen atom at corner of $Si_2O_5(OH)^{3-}$ to form 1:1 metal phyllosilicate as illustrated in **Figure 2.5.** Moreover, phyllosilicate has the characteristic structure, the metal ion in octahedral layer acting as the Lewis acid sites and surface OH groups act as the Bronsted acid site. It is an interesting catalyst in the studied reaction.

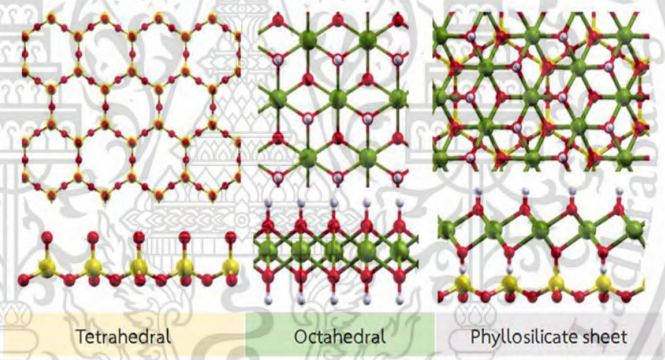

Figure 2.5 The phyllosilicate structure (a) Tetrahedral layer. (b) Octahedral layer and (c) 1:1 metal phyllosilicate structure[23].

2.6 Literature reviews

This part is summarized the literature research which related to catalytic hydrogen transfer of furfural to gamma-valerolactone.

Sitthisa et.al. (2019) [24] Furfural hydrogenation over Cu/SiO_2 has been described. Furfuryl alcohol was the major byproduct of carbonyl hydrogenation. The results show furfural adsorption on the Cu surface in η^1 (O)-aldehyde. A initial H attack on the O atom

of the carbonyl group may result in the creation of a hydroxyalkyl species. The energy barrier would be lower, according to the DFT calculations..

Román-Leshkov et.al. (2013) [8] The domino reaction was researched in order to create GVL from furfural. A mixing of Lewis and Brønsted acids solid catalysts. Lewis acid Zr-Beta and aluminosilicate with MFI as a Brønsted acid catalyst The results showed a 98% conversion and a 78% GVL yield. Furfuryl alcohol was synthesized utilizing a Lewis acid catalyst-assisted transfer hydrogenation using 2-butanol as the hydrogen donor. The Brønsted acid was then used to convert furfuryl alcohol and butyl levulinate to levulinate acid and butyl levulinate. The levulinate acid and ester were then transferred hydrogenated under Lewis' acid catalyst to get 4-hydroxypentanoates. Finally, following lactonization, GVL was produced. Importantly, the Lewis and Brnsted acids had a considerable effect on GVL product yields in the study

Weibin Fan et.al. (2016) [7] studied the combination of Au/ZrO_2 with ZSM-5 for the conversion of Hemicellulose and furfural to γ-valerolactone. The case of furfural as a reactant for GVL production required active metal and acid site. The screening solid acid catalysts for combination with Au/ZrO_2, ZSM-5 showed the highest yield of GVL (80.4 %). Due to Au/ZrO_2 as a Lewis acid pair and ZSM-5 showed large amounts of medium-strength acid sites. The synergistic effect of the both acid can be improved the catalytic performance under mild condition. For the integrate conversion of hemicellulose into GVL via a two-step process. A 61.5% overall yield of GVL was obtained from Hemi-Cellulose. This provides a simple route for synthesizing GVL.

Haryo Pandu Winoto et.al. (2016) [6] A bifunctional Sn-Al-Beta zeolite with isolated Lewis and Brnsted acid sites was investigated. They observed that Sn-Al-Beta 7 had the highest GVL yield due to the higher concentration of framework Sn sites and the moderate Brønsted acidity. Furthermore, the proximity of the Brønsted and Lewis acid site has a synergistic effect on GVL formation. It was also discovered that the degree of

dealumination and the tin-incorporation method had a substantial influence on the acid characteristics and selectivity of the catalyst.

B. Srinivasa Rao et.al. (2021) [25] reported the bifunctional mesoporous silica catalysts containing Zr and tungstophosphoric acid (TPA) prepared by varying the location of TPA and ZrO_2 inside and outside the pores of SBA-15. The catalyst containing ZrO_2 inside the mesoporous channels of SBA-15 and TPA distributed outside performed better, 81% of GVL yield. Because the catalysts contain both Brønsted and Lewis acids, a suitable ratio is required to produce the GVL. Furthermore, the interaction between the catalyst and the hydrogen donor was essential to the TPA/ZrO_2-SBA-15 catalyst's high GVL yield. As a result, the activity of transfer hydrogenation is influenced by the interactions of the hydrogenating alcohol and the acid–base properties of the catalyst.

Jian He Dual et.al. (2020) [26] studied the acidic mesoporous KIT silicates in one-pot production of γ-valerolactone from biomass. Zr-KIT-5(10) showed 93.8% EL conversion with 91.4% GVL selectivity at 180 °C, 6 h with 2- propanol as H-donor. In contrast, the conversion of biomass-based furfural to GVL 40.1% yield of GVL and 21.2% yield of IPL at 180 °C for 6 h. Due to Zr-incorporated mesoporous silica (KIT-5) catalysts was presented both Lewis and Brønsted acid sites and the large number of acidic sites and easy access of active sites to interconnected pores. The higher acidic and L/B ratio are influence for conversion and GVL production.

Hongwei, et. al (2019) [21] studied the one-pot cascade transformation of biomass-derived furfural to -valerolactone using a combination of Zr-HY and Al-HY zeolite catalysts. They compare two catalyst series Zr-beta and Zr-HY zeolite. It was discovered that Zr-HY zeolite has more activity than Zr-Beta because it has bigger pore size and stronger Lewis acidic sites. Furthermore, when Al-HY and Al-Beta zeolites were compared, they discovered that Al-HY zeolites were more efficient as Brønsted acid than Al-Beta because they converted furfuryl ether to levulinate ester rather than b-angelica lactone. So, when

the physical mixing between Zr-HY Lewis acid and Al-HY Bronsted acid catalysts, Zr-HY-15-20 (Si/Al ratio=15, Si/Zr ratio=20) and Al-HY-6 (Si/Al ratio=6) demonstrated outstanding activity for this process., with 85% GVL yield after only 5h at120°C.

Yu-Chuan L. et. al. (2018) [27] reported the highly selective silica-supported copper catalysts derived from copper phyllosilicates for hydrogenation of adipic acid (AA) to 1,6- hexanediol. The ammonia evaporation hydrothermal method was used to prepared CuPS. 25 wt% of ammonia aqueous solution and Cu $(NO_3)_2 \cdot 3H_2O$ were mixed in 70 mL of deionized water under vigorous stirring. First step 2.5 grams of colloid silica (LUDOX® HS30, Aldrich) was then added into the mixture solution and controlled pH around the range of 11 to 12 and stirred for 24 h. After that suspension was heated in a water bath at 80°C to allow ammonia evaporation and transfer into autoclave for hydrothermal and treated at 150°C for 24 h. The precipitates were filtered, washed with deionized water three times, dried at 120 °C for 4h, and calcined at 400 °C for 4h. They studied in a batch reactor was used to studied the catalytic performance. In addition, the $Cu^+/ (Cu^{0+} Cu^+)$ ratio can be generate by the stronger Cu- silica interaction. the intrinsic activity of hydrogenation improved by the $Cu^+/(Cu^{0+}Cu^+)$ ratio, the amounts of Cu^0 and Cu^+ sites, and the reduction condition.

Dong, Zhu et al. (2017) [28] prepared copper phyllosilicate catalyst for the synthesis of biofuel 2-methylfuran from furfural. They found that the acid increased with the increase of Cu loading and the total acidity of the sample surface increased with the increase of the Cu–Si molar ratio. The excess acid sites of the catalyst promoted the formation of a GVL by-product. By the acid sites could obtain from two distinct locations of phyllosilicate (1) coordinatively unsaturated metal (II) sites near the edges/surfaces of phyllosilicate act as Lewis's acid and (2) surface OH groups act as Brønsted acid.

Ya-Ju Tsou et al. (2020) [17] studied Hydrophobic Copper Catalysts Derived from Copper Phyllosilicates in the Hydrogenation of Levulinic Acid to γ-Valerolactone. They

found a reduction–silylation–reduction process was developed to prepare hydrophobic Cu catalysts derived from CuPS induced acidity of catalysts. Hydrophobization by OTS grafting has advantages in enhancing GVL yields and in limiting Cu sintering. High LA conversion (95.7%), GVL yield (85.2%), and stability (3 cycles with a 7.5% loss of initial activity) were obtained at a mild reaction condition.

In summary, for improve GVL production by using catalytic transfer hydrogenation of furfural. The conversion and GVL production depend on acidity and appropriate ratio of Brønsted and Lewis acid sites on the surface catalyst. Therefore, tuning the suitable acidity on heterogeneous catalysts is the key issues for the catalytic transfer hydrogenation of furfural to GVL.

CHAPTER 3

EXPERIMENTAL

3.1 Chemicals

Details of the chemical used to prepare catalyst and used for the reaction study have been summarized in **Table 3.1**

Table 3.1 List of the chemicals for catalysts preparation and catalytic testing.

Chemical	Grade of purity	Supplier
Ammonia Solution (NH_4OH)	28-30%	CARLO ERBA
Copper (II) nitrate trihydrate ($Cu(NO_3)_2 \cdot 3H_2O$)	99.50%	CARLO ERBA
Maganese (II) nitrate tetrahydrate ($Mn(NO_3)_2 \cdot 4H_2O$)	98.50%	CARLO ERBA
Zinc (II) nitrate hexahydrate ($Zn(NO_3)_2 \cdot 6H_2O$)	97.50%	CARLO ERBA
Furfural	99.00%	Sigma Aldrich
Isopropanol	99.90%	CARLO ERBA
Methanol	99.80%	CARLO ERBA
Toluene	40.00%	CARLO ERBA
LUDOX® AS-40 colloidal silica	98.50%	Sigma Aldrich
Air zero grade das	99.99%	UIG
1% Ammonia in Helium	99.99%	Linde
Helium gas	99.99%	PRAXAIR
Hydrogen gas	99.99%	UIG
1% Hydrogen gas in Argon	99.99%	PRAXAIR
10% Hydrogen gas in Argon	99.99%	PRAXAIR
Nitrogen gas	99.99%	UIG
Distilled water		

3.2 Catalysts preparation

3.2.1 Synthesis of 10 wt.% copper phyllosilicate catalyst (10%CuPS)

The 10 wt.% copper phyllosilicate catalyst (10%CuPS) was prepared by dissolved 2.536 g of copper (II) nitrate trihydrate ($Cu(NO_3)_2•3H_2O$) in 60 mL of distilled water. Then, 7.85 mL of ammonia solution was added and continuously stirred for 10 min with the ratio of [Cu]:[NH_3] = 1:12. After that, 11.60 mL of colloidal silica sol. (40 wt.%) was added and stirred for 24 h at room temperature (pH≈11). The suspension was stirred at 80°C in a oil bath to evaporation ammonia until pH value decreased from 11 to 7. The remaining mixture was hydrothermal at 150°C for 24 h. After that, the solution was filtered and washed with distilled water, and dried at 60°C for 24 h. The obtained solid was calcination in a tube furnace at 400°C with a heating rate of 1°C/min under 60 mL/min of air flow for 4 h. The obtained solid was denoted as 10%CuPS catalyst.

3.2.2 Synthesis of 20 wt.% copper phyllosilicate catalyst (20%CuPS)

The 20 wt% of copper phyllosilicate catalyst (20%CuPS) was prepared by dissolved 5.703 g of copper (II) nitrate trihydrate ($Cu(NO_3)_2•3H_2O$) in 60 mL of distilled water. Then, 12.64 mL of ammonia solution was added and continuously stirred for 10 min with the ratio of [Cu]:[NH_3] = 1:12. After that, 11.60 mL of colloidal silica sol. (40 wt%) was added and stirred for 24 h at room temperature (pH≈11). The suspension was stirred at 80°C in a water bath to evaporation ammonia until pH value decreased from 11 to 7. The remaining mixture was then hydrothermal at 150°C for 24 h. After that, the solution was filtered and washed with distilled water, and dried at 60°C for 24 h. The obtained solid was calcination in tube furnace at 400°C with the heating rate of 1°C/min under 60 mL/min of air flow for 4 h. The obtained solid was denoted as 20%CuPS catalyst.

3.2.3 Synthesis of 30 wt.% copper phyllosilicate catalyst (30%CuPS)

The 30 wt.% copper phyllosilicate catalyst (30%CuPS) was prepared by dissolved 15.2078 g of Copper (II) nitrate trihydrate ($Cu(NO_3)_2•3H_2O$) in 60 mL of distilled water. Then, 47.60 mL of ammonia solution was added and continuously stirred for 10 min with the

ratio of [Cu]:[NH_3] = 1:12. After that, 11.60 mL of colloidal silica sol. (40 wt%) was added and stirred for 24 h at room temperature (pH≈11). The suspension was stirred at 80°C in a water bath to evaporation ammonia until pH value decreased from 11 to 7. The remaining mixture was then hydrothermal at 150°C for 24 h. After that, the solution was filtered and washed with distilled water, and dried at 60°C for 24 h. The obtained solid was calcination in a tube furnace at 400°C with the heating rate of 1°C/min under 60 mL/min of air flow for 4 h. The obtained solid was denoted as 30%CuPS catalyst.

3.2.4 Preparation of reduced copper phyllosilicate catalysts

copper phyllosilicate catalysts were reduced at 250°C with a heating rate 10°C/min under 30 mL/min of H_2 flowing for 2 hours in tube furnace. Approximately, 0.2 g of catalyst was packed in to 0.6 nm inner diameter quartz tube then set up into furnace.

3.2.5 Preparation of physical mixing 30 wt.% copper phyllosilicate catalyst (Physical mixing 30%CuPS)

The Physical mixing 30 wt% Copper Phyllosilicate Catalyst (Physical mixing 30%CuPS) using ratio of 1:1 were prepared the solid 30%CuPS catalyst of 0.1 g and the solid 30%CuPS reduced catalyst of 0.1 g. Both catalysts were combined by grinding. The obtained solid was denoted as Physical mixing 30%CuPS catalyst.

3.2.6 Preparation of 1%Mn_2O_3/30CuPS was prepared by incipient wetness impregnation method

The 30%CuPS reduced catalyst was taken as a support, dissolved Manganese (II) nitrate tetrahydrate ($Mn(NO_3)_2$•$4H_2O$) 0.1352 g in 5.4 mL of distilled water. After that was added into 30%CuPS and then dried catalyst. Finally, calcination at 400 °C for 4 h. The catalyst was denoted as 1%Mn/CuPS

3.2.7 Preparation of 1%ZnO/30CuPS was prepared by incipient wetness impregnation method

The 30%CuPS reduced catalyst was taken as a support, dissolved Zinc (II) nitrate hexahydrate ($Zn(NO_3)_2$•$6H_2O$) 0.213 g in 8.4 mL of distilled water. After that was added into

30%CuPS and then dried catalyst. Finally, calcination at 400 °C for 4 h. The catalyst was denoted as 1%ZnO/CuPS

3.3 Catalyst Characterization

3.3.1 X-ray Fluorescence (XRF)

The chemical composition of catalysts can be also determined by a wavelength - dispersive X-ray fluorescence spectrometry (WD-XRF). The sample is prepared by mixing 4.5 grams of boric acid and 0.5 grams of catalyst followed by manual grinding. The mixture was packed onto the sample holder and then compressed at 150 kN. The sample was placed in the sample chamber. CuKα was employed as a source for the measurement with 50 kV. 60 mA.

3.3.2 X-ray Diffraction (XRD)

X-ray diffraction methods are the most effective methods for determining the crystal structure of materials. The sample was packed onto the sample holder and then press surface smooth. X-ray tube Copper is employed as a source for the measurement with 40 kV, 30 mA. Scan range 20-80 deg, step size 0.0200 deg.

3.3.3 N_2 Physisorption (BET)

Specific surface area of a catalyst was measured by an Autosorb (Quantachrome) instrument. Each sample (weighed approximately 0.1g) was degassed at 300°C for 12 h prior to analysis. After that, nitrogen gas was adsorbed on the surfaces of the sample at -196°C. The adsorbate pressure was fixed at 1 torr, the equilibration time of 3 min at each point, and the scaled tole, the equilibration time of 3 min at each point, and the scaled tolerances were set zero. The surface area was analyzed employing BET equation. The BJH pore size distribution was also calculated.

3.3.4 H_2-Temperature programmed reduction by hydrogen gas (H_2-TPR)

The reducibility property of metal contents can be determined by a temperature programmed reduction by H_2 gas (H_2-TPR). The measurement was performed in a quartz tube connected with a thermal conductivity detector (VICI). Prior to an analysis, the samples (0.015 g approximately) was activated in air (flow rate of 30 mL•min^{-1}) from room temperature to 400°C at a heating rate 5°C min^{-1}, the system was thermally cooled to room temperature in a nitrogen gas environment (flow rate of 30 mL•min^{-1}). The gas was then changed to 10% H2 in Ar at a heating rate of 10oC min-1 from 35 to 900°C. Because CuO is reduced stoichiometrically and totally to Cu and H_2O, the TCD signal was calibrated using a known mass of CuO as a reference. After each run, the internal TCD calibration was conducted by pulsing 10% H_2/Ar in the fixed loop. The amount of moles of copper is equal to the reduction profile of CuO and the utilization of hydrogen. Metal loading is measured in mmol of H_2 used per mass of a catalyst (mmol H_2/g).

3.3.5 NH_3-Temperature Programmed Desorption (NH_3-TPD)

The acid sites of the catalyst were identified using temperature-programmed desorption of ammonia (NH_3-TPD) measurement. Sample was preheated in the flow of air zero (30mL/min) at 400°C for 1 h and evacuated. After that, it was exposed to 20 kPa of 1% NH_3/He gas at 30°C until saturation coverage was reached. Afterward, the sample was flushed with He at room temperature for 40 min, the temperature was then increased at a linear rate of 10°C /min from 50 to 900°C under vacuum.

3.3.6 X-ray photoelectron spectroscopy (XPS)

X-ray photoelectron spectroscopy (XPS) is a helpful measuring technique since it reveals which elements are present in a film and to which elements they are linked. This means that if you have a metal oxide and want to know whether it is in the oxidation state, you may use XPS to determine that ratio. However, the equipment will only probe a sample 20 nm deep.

3.3.7 Pyridine-adsorbed infrared spectroscopy (Py-IR)

The Brønsted and Lewis acid sites were analyzed using pyridine- adsorbed infrared spectroscopy (Py-IR, Thermo Scientific Nicolet iS50 spectrometer. Briefly, the sample was pretreated to 200 °C. Once it was cooled down to 150 °C and exposed to pyridine vapor. After that, excess pyridine was removed under a vacuum (5.2×10^{-3} Pa) for 1 h. Finally, the sample was heated to 200 °C (5 °C/min) and the FTIR spectra were recorded

3.3.8 In situ time-resolved X-ray adsorption near-edge structure (in situ TR-XANES)

The experiments were performed at BL5.2: TRXAS, Synchrotron Light Research Institute (SLRI), Thailand. An energy dispersive monochromator and position sensitive detector was employed to perform XANES measurement. The Cu K-edge XANES was collected using the integration time of 2000 ms with an average of 10 scans. The oxidation state of copper composition was estimated by Linear Combi- nation Fitting (LCF) of XANES spectra over Athena software using Cu foil, Cu_2O, CuO and $CuSO_4$ as a standard.

3.3.9 Transmission electron microscopy (TEM)

The Cu nanoparticle size was measured by transmission electron microscopy (TEM) on a JEM-2010. The sample was dispersed in ethanol and deposited on copper grids coated with transparent carbon foil and dried in vacuum

3.4 Catalysts Activity test

The liquid phase hydrogenation of furfural was carried out in a 100 ml of batch type autoclave reactor as show in **Figure 3.1**. Typically, 200 µL of furfural was mixed with 10 mL of isopropanol in a volumetric flask and then put it in the Teflon liner tube in an autoclave reactor. Approximately 200 mg of catalyst was added to the reactor and then closed. After that. the reactor was purged 3 times with N_2 to replace the air inside. Then, 10 bars were put of N_2 into the reactor top prevent the evaporation of gas product. After

that, the reactor was heated to the reaction temperature (160°C). The stirring speed was set at 600 rpm. After reaction, the liquid products were separated from the catalyst by centrifugation. The liquid product was mixed with external standard and analyzed by gas chromatography using RTX-5 capillary column.

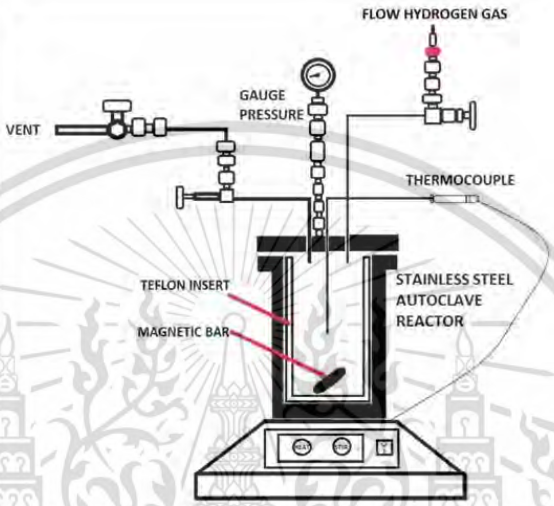

Figure 3.1 Schematic diagram of batch reactor for liquid-phase hydrogenation of furfural to GVL.

CHAPTER 4

RESULTS AND DISCUSSION

This chapter shows the results and discussion, which divided in three parts. In the first part, the effect of copper loading on CuPS catalysts (10-30%CuPS) and Cu species (Cu^0, CuO) were studied in the catalytic transfer hydrogenation of furfural to GVL. The CuPS were prepared by ammonia evaporation hydrothermal method. The characteristic and catalytic properties of CuPS catalysts were determined by several techniques such as XRD, H_2-TPR, TEM, XPS, XRF, N_2 adsorption-desorption, NH_3-TPD, Pyridine-IR and XANES. In the second part, the physical mixing between 30%CuPS-R and 30%CuPS by various ratios (70: 30, 50:50, and 30:70) were investigated. In the third part, the effect of metal oxide doping (ZnO, Mn_2O_3) on 30%CuPS-R catalysts were studied in the catalytic transfer hydrogenation of furfural to GVL. The catalysts were prepared by incipient impregnation method.

Part 1

Effect of copper loading and Cu species (Cu^0, CuO) on copper phyllosilicate catalysts for the catalytic transfer hydrogenation of furfural to GVL.

4.1 Characterization of catalysts

4.1.1 X-ray diffraction pattern, XRD

The crystal structure and phase compositions of CuPS catalysts were determined by XRD techniques. The XRD patterns of CuPS catalysts were compared with the literatures or JCPDS databases. The XRD spectra of CuPS catalysts are shown in **Figure 4.1.** The diffraction peak at 2θ = 22.0° was observed in all catalysts. This is the characteristic peak of amorphous silica. The diffraction peaks at 2θ = 30.8°, 35.0°, 57.5°, and 62.4° corresponding to the pattern of chrysocolla ($Cu_2Si_2O_5(OH)_2$) were found on CuPS catalysts after calcination at 400 °C as shows in **Figure 4.1 A**. The intensity peaks of copper became more intense when copper loading increased from 10-30%, indicating increasing of formation of octahedral layered structure.However, the characteristic of CuO peak could not be observed on the calcined CuPS catalysts suggesting to highly dispersion of copper on the phyllosilicate structure.

Figure 4.1 B shows the XRD patterns of CuPS catalysts after reduction at 250 °C. The diffraction peaks at 2θ = 43.2°,50.4°, and 74.1°,which were assigned to metallic Cu^0 (111), (200), and (220) plans, respectively were clearly observed. Furthermore, The estimated Cu particle size calculated from Scherrer's equation by using FWHM of Cu (111) peak were 3.3, 4.7, and 5.4 nm for 10%CuPS-R, 20%CuPS-R, and 30%CuPS-R, respectively. It was found that copper particle size increased when increased copper loading Suggesting that high copper loading trends to occur agglomeration of copper particles.

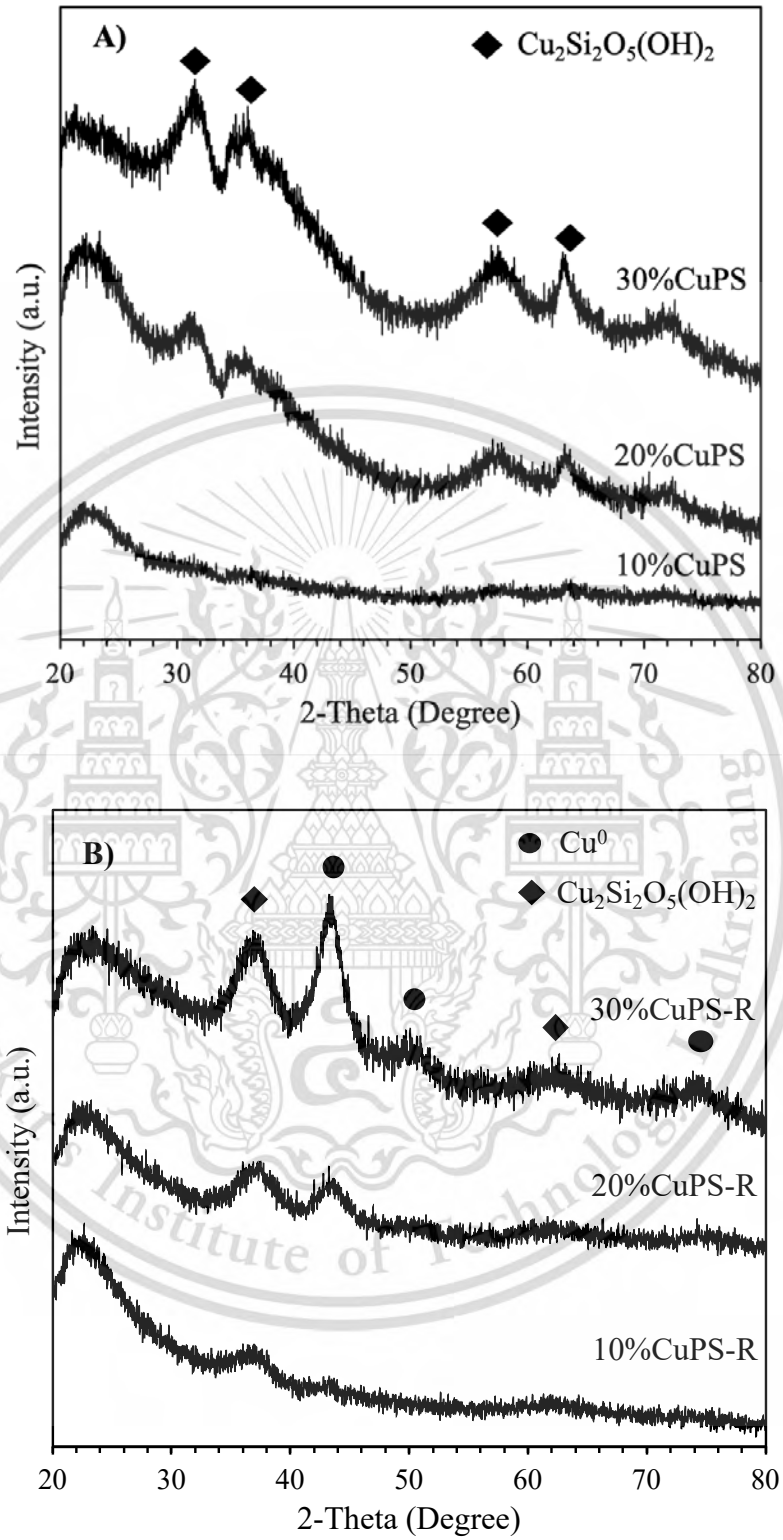

Figure 4.1 XRD patterns of CuPS catalysts A) after calcination at 400 °C; B) after reduction at 250 °C

4.1.2 H_2 Temperature program reduction (H_2-TPR)

The reduction behavior and reducibility of CuPS catalysts were determined by H_2-TPR technique. **Figure 4.2** shows the H_2-TPR profiles of CuPS catalysts. Only one reduction peak in the range of 150-220 °C , which was the reduction of CuO to metallic Cu^0, were observed. Generally, reduction of CuPS occupies two reduction stages: i) Cu^{2+} to Cu^+, and ii) Cu^+ to Cu^0. Both stages shows only one reduction peak at temperature lower than 240 °C [29,30]. Considering the maximum temperature reduction, the maximum reduction peak wasshifted from 220 °C to 233 °C when enhance the Cu loading from 10-30%. since It might be because of different copper loading and copper dispersion. According to the literatures, the highly dispersed of CuO particles or small CuO particles were easily reduced to metallic Cu^0 than a large CuO particle size The hydrogen consumption or reducibility is reported in **Table 4.1**. The hydrogen consumption increased from 1.44 to 4.77 mmol/g when increased copper loading from 10% to 30%. To estimate the H_2 consumption (by integration of the TPR peak compared with the theoretical H_2 consumption (determined by XRF), the results showed that the actual H_2 consumption was lower than the theoretical values for the full reduction of copper species to Cu^0. This suggests that Cu^{2+} species in phyllosilicate might not be fully reduced to metallic Cu^0. There were some Cu^+ species on the structure, which were formed by the co-reduction of copper phyllosilicate and well-dispersed CuO [31].

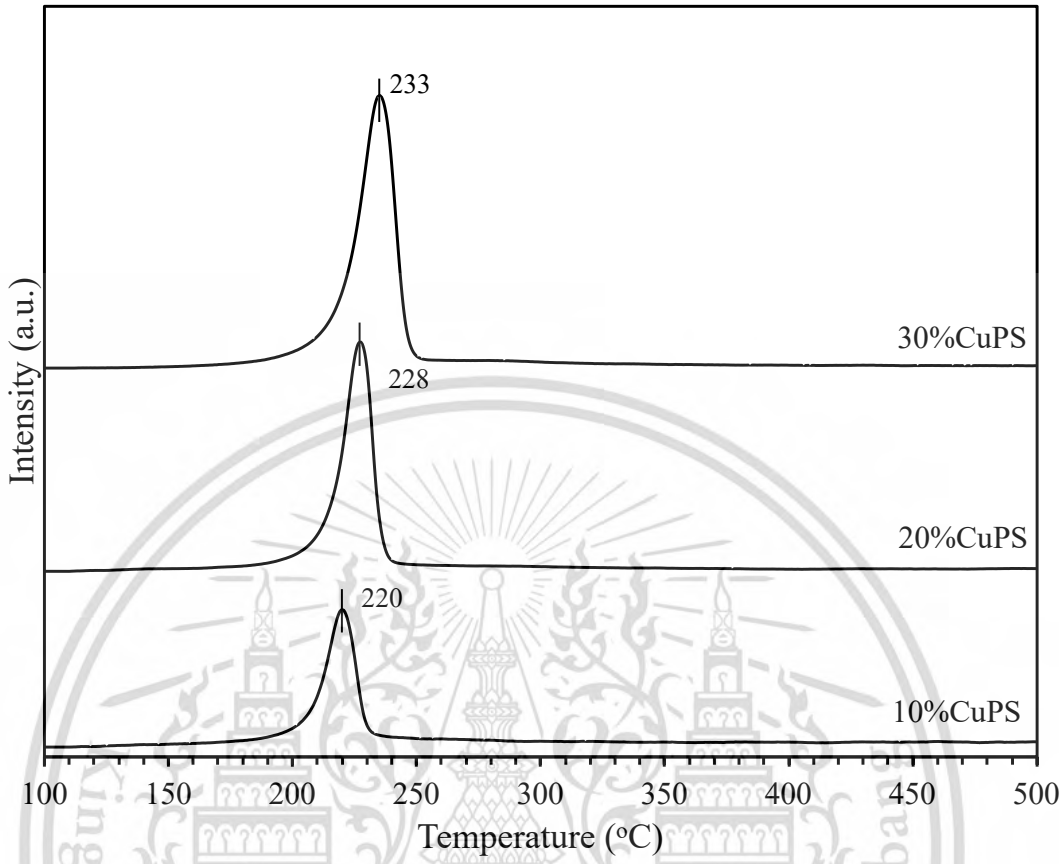

Figure 4.2 H_2- TPR profile of CuPS catalysts.

4.1.3 N_2O Temperature program reduction (N_2O-TPR)

To estimate the dispersion and quantify the surface concentration of Cu^0, reduced CuPS was subjected to dissociative N_2O adsorption followed by subsequent TPR test to acquire amounts of consumed H_2 in the reduction of N_2O-oxidized as shows in **Figure 4.3.** The second H_2-TPR profile showed a broad peak at approximately 155 °C for each sample. The H_2 uptake of A_2 can be used to calculate the concentration and surface area of accessible Cu^0 with the assumption that the specific surface area of Cu is 1.46 x 10^{19} atom/m^2. The dispersion (D_{cu}) of Cu calculated by (2 x A_2/A_1) x 100%.

The calculated Cu dispersion were 78.9%, 72.1%, and 69.8% for 10%CuPS, 20%CuPS, add 30%CuPS respectively. It is well known that high dispersed CuO with small particle sizes can be more facilely reduced to metallic Cu^0 than did the bulk CuO with larger sizes[32]. Therefore, the copper particle size was in the order 10%CuPS > 20%CuPS >30%CuPS.

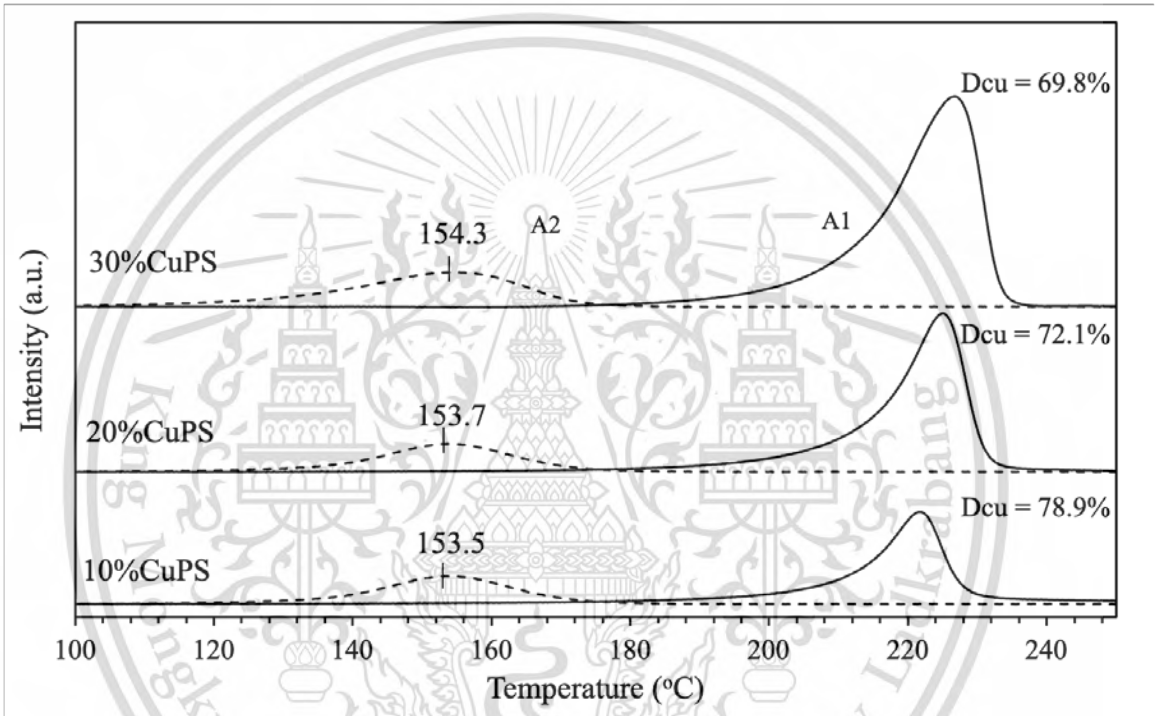

Figure 4.3 N_2O -TPR profile of CuPS catalysts.

4.1.4 Physiochemical properties of CuPS catalysts.

Table 4.1 The physical properties of CuPS catalysts

Catalyst	Cu loading (wt.%)[a]	N_2-adsorption desorption		Theoretical H_2 consumption (mmol/g)[a]	H_2 Consumption from H_2-TPR (mmol/g)
		S_{BET} (m^2/g)	Average pore size diameter (nm)		
10%CuPS	10.1	272	12.3	1.59	1.44
20%CuPS	19.0	418	6.4	2.99	2.91
30%CuPS	30.8	620	3.4	4.84	4.77

[a] determined by XRF,

[b] Theoretical H_2 consumption calculated by considering the Cu loading measured by XRF.

The copper loading, BET surface area, average pore size diameter, and H_2-consumption of CuPS catalysts are summarized in **Table 4.1** The actual amount of copper loading on CuPS catalysts determined by XRF were consistent with the desired amount of Cu loading in catalysts. The BET surface area increased from 272 to 620 m^2/g when copper loading increased from 10-30%. I Because of increasing of Cu loading trends to form theCu octahedral layer in phyllosilicate structure as evidenced by XRD.Furthermore, all CuPS samples show type IV N_2 adsorption-desorption isotherm **(Figure 4.4)**, indicating the mesoporous material with the average pore sizes diameters calculated by the Barrett-Joyner-Halenda (BJH) equation in the range of 3-13 nm. The small mesopores around 3 nm was associated with the narrow parallel plates of CuPS whereas the bigger mesopores (6.4 and 12.4 nm) was associated with the empty space of agglomerated copper particles[27].

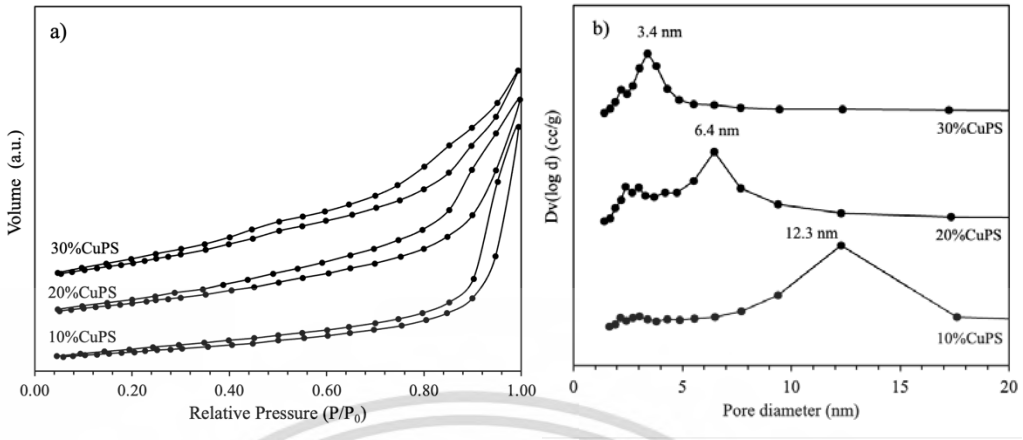

Figure 4.4 a) Adsorption- desorption isotherm and b) pore diameter of CuPS catalysts

4.1.5 Transmission Electron microscope (TEM)

Figure 4.5 shows the TEM images of 10%CuPS, 20%cuPS, and 30%CuPS catalysts after calcination at 400 °C and reduction at 250 °C with the corresponding the histogram of Cu particle size distribution of all CuPS after reduction. The morphology of CuPS after calcination at 400 °C exhibited the sheets and layered structure of phyllosilicate. Moreover, the layer structure forming was clearly observed when increasing Cu loading from 10-30%. The presence of ill-crystallized phyllosilicate was claimed. After reduction, the light gray silica supports were identified along with highly dispersed dark spherical assignable to metallic copper species. It was apparent that copper particles were uniformly dispersed onto the silica support in all catalysts. The average copper particle sizes were 3.2, 4.3 and 5.0 for 10%CuPS-R, 20%CuPS-R, and 30%CuPS-R respectively.

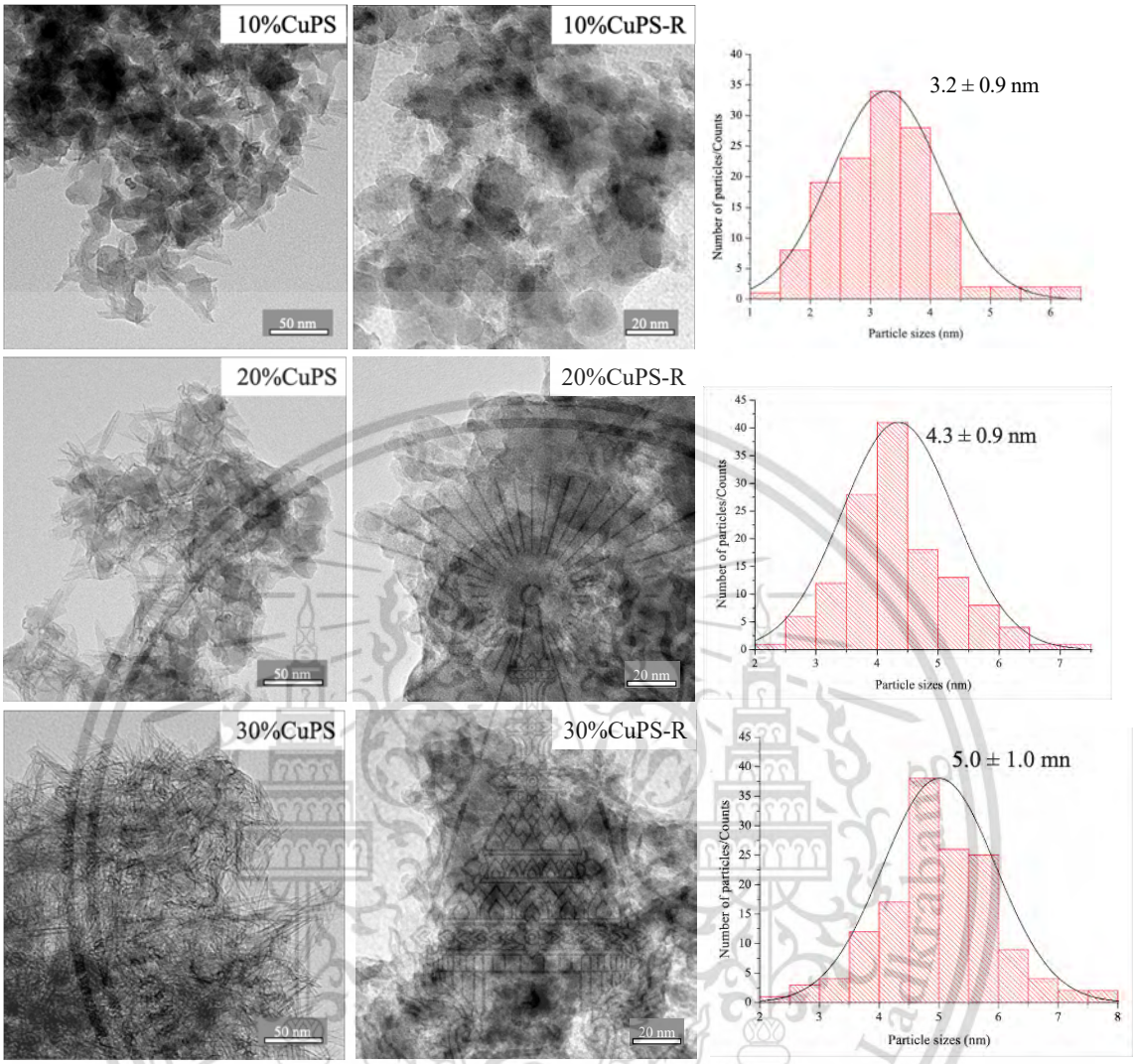

Figure 4.5 TEM image of CuPS after calcination, reduction, and particle size distribution histogram of CuPS catalysts.

4.1.6. X-ray absorption near edge structure (XANES)

To investigate the geometry, and Cu species in CuPS catalysts after calcination and reduction, the samples were characterized by XANE techniques and the results show in **Figure 4.7**. The Cu edges energy for Cu standard were 8,978.9 for Cu foil, 8,979.9 for Cu_2O, 8,990.5 for CuO (square planar), and 8,993.2 for $CuSO_4$ (octahedral). The geometry of Cu as shown is **Figure 4.6**. All of CuPS shows the characteristic edge energy absorption around

8992 eV. It is worth noted that the values are between the Cu edge energy of $CuSO_4$ (8993.2eV) and^{2+}CuO (8890.5 eV). As a result, the calcined CuPS samples are expected to have an octahedral and square planar combination. The line shape of all CuPS looks like $CuSO_4$. This indicating that the Cu^{2+} species is major species to form octahedral coordination in the chrysocolla structure.

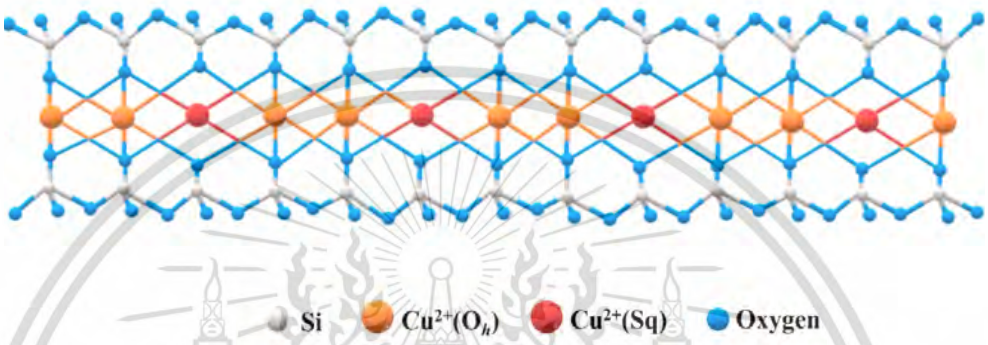

Figure 4.6. The demonstration of Cu^{2+}(octahedral) and Cu^{2+}(square planar) after the calcination at 400 °C [33].

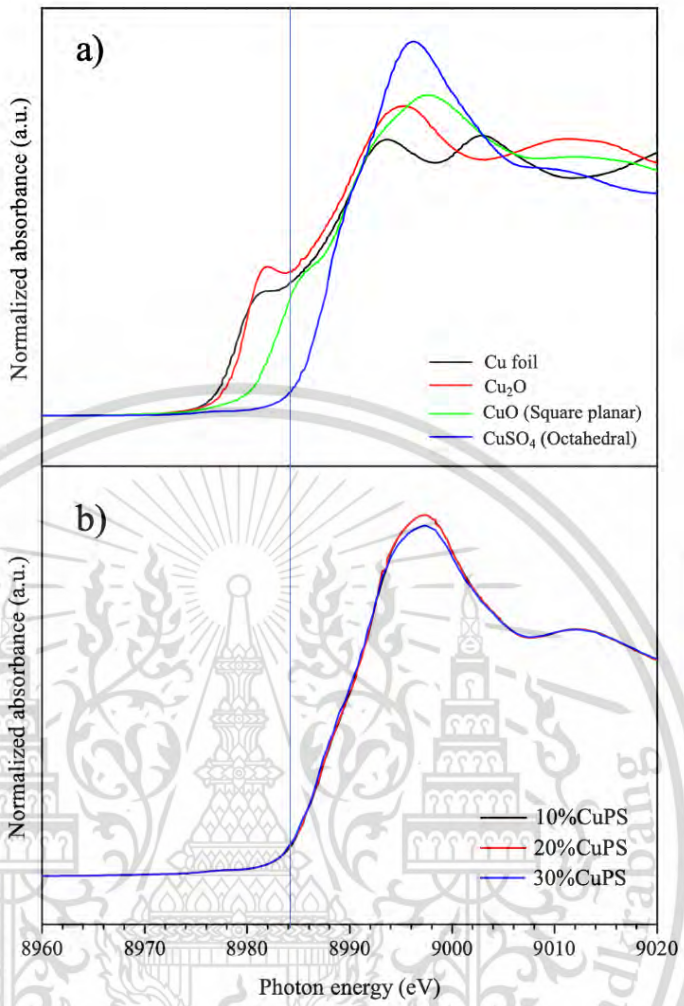

Figure 4.7 Cu K edge XANES spectra of a) Cu standard and b) CuPS after calcination at 400 °C for 2 h.

To investigate the oxidation state and local structure of copper species during the reduction condition, the in-situ Temperature program-XANES under 10%H_2/N_2 was perfprmed and the results show in **Figure 4.8**. According to the Cu K edge in-situ XANES spectra, the line shape of all CuPS like Cu^{2+} (square planar) appearance at the 30 ° C. When the temperature increased from 30 °C to 250 °C the line shape of all CuPS were change from Cu^{2+}(square planar) to nearly metallic Cu^0 or Cu foil.

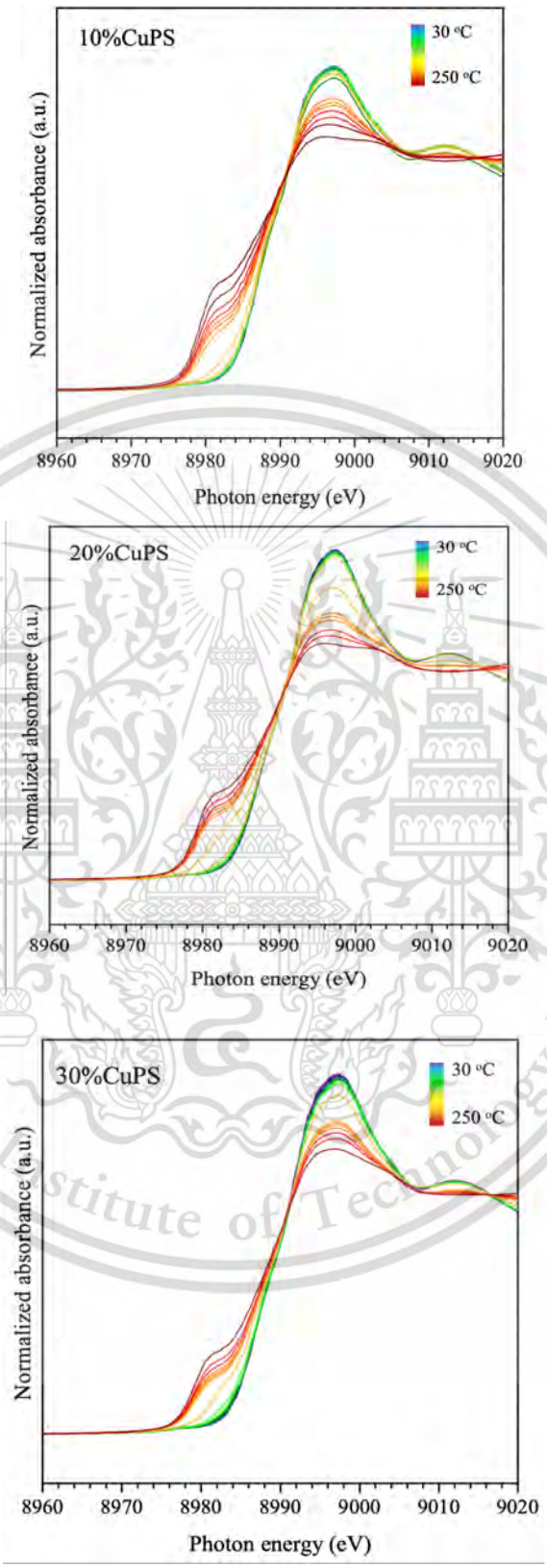

Figure 4.8 Cu K edge in-situ XANES spectra of CuPS

According to the linear combination fitting (LCF) using the first derivatives of reference compounds corrected for experimentally observed energy shifts and plotted as shown in **Figure 4.9**. All of CuPS showed the Cu^{2+}(Octahedral) species were decreased at temperature around 50–220 °C. In response to such decrease, Cu^{2+}(square planar) species gradually increased, suggesting that the dehydroxylation of Cu^{2+}(Octahedral) species to Cu^{2+} (square planar) was promoted under hydrogen. It is possible that the hydrogen could reversibly dissociate Si-O-Cu-O- Si forming internal Si-OH and H-Cu-O-Si. The latter species may also react with the adjacent HO-Cu-O-Si, liberating H_2 and Cu-O-Cu [33]. in situ TR-XANES experiment has suggested that the coordination of Cu^{2+} has been modified under hydrogen without change in the oxidation state.

The reduction step by step from the reduction of Cu^{2+} to Cu^{+} species could be initially observed at 210 °C, followed by the formation of Cu^0 at 230 °C. These two species were evolved along with the decreases in Cu^{2+} (Octahedral) and Cu^{2+} (square planar) species. This observation suggests that the Cu^{2+} (Octahedral) species would be partially reduced to Cu^{+} at below 210°C, presumably due to a strong interaction of Cu^{+} in octahedral geometry with the SiO_2 layers. Nevertheless, some of Cu^{+} could be further reduced to Cu^0, as observed by a decrease in Cu^{+} fraction at > 220 °C.

The fraction Cu species from LCF as shown in **Figure 4.9 and Table 4.2.** Initially, at 30 °C shown when copper loading increased fraction of Cu^{2+} (square planar) was increased from 37.8 to 45.8% while Cu^{2+}(octahedral) was decreased from 62.2 to 54.2%. After heated up to 250 °C. Both of Cu^{2+} species were not observed. It could be Cu^{2+} was reduced to Cu^{+} and Cu^0 species. For the fraction of Cu^{+} and Cu^0 after reduction at 250 °C in order to 10%CuPS (17.2%) > 20%CuPS (11.2%) > 30%CuPS (8.3%) for Cu^{+} species and 30%CuPS (91.7%) > 20%CuPS (88.8%) > 30%CuPS (82.8%) for fraction of Cu^0 species

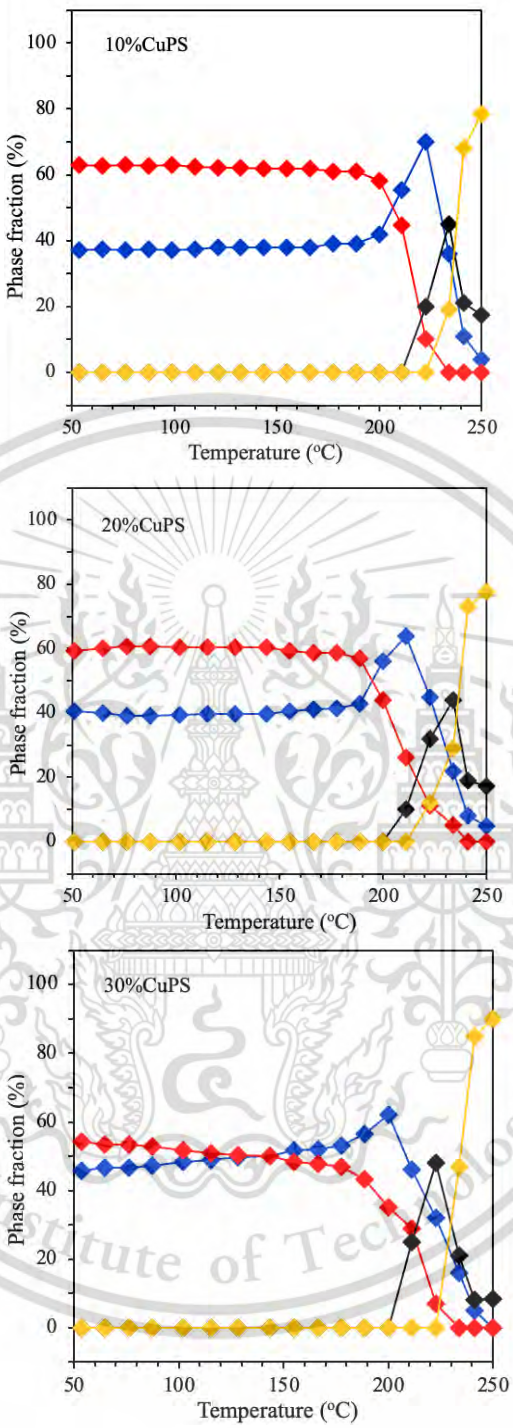

Figure 4.9 The fractions of Cu^{2+} species (◆) Cu^{2+} Square planar, (◆) Cu^{2+} Octahedral, (◆) Cu^{0}, (◆) Cu^{+} obtain from linear combination fitting (LCF).

Table 4.2. Fraction of Cu species

Catalyst	Cu fraction (%)			
	30 °C		250 °C	
	Cu^{2+} (square planar)	Cu^{2+} (octahetral)	Cu^{+}	Cu^{0}
10%CuPS	37.8	62.2	17.2	82.8
20%CuPS	39.4	60.6	11.2	88.8
30%CuPS	45.8	54.2	8.3	91.7

4.1.7. X-ray Photoelectron Spectroscopy (XPS)

The electronic states and surface composition of CuPS catalysts were identified by XPS analysis. **Figure 4.10** illustrates the XPS spectra of Cu 2p calcined and reduced CuPS catalysts. For calcined CuPS catalysts, the Cu $2p_{3/2}$ spectra show the main peak at binding energy at 935.9 eV for 10%CuPS, 936.2 for 20%CuPS, and 936.5 eV for 30%CuPS. This peak was attributed to dispersed Cu^{2+} species on phyllosilicate structure [34,35]. After reduction, the XPS spectra of Cu $2p_{3/2}$ for reduced CuPS catalysts shift to lower binding energy at 932.5 eV for 10%CuPS, 932.7 eV for 20%CuPS, and 932.9 eV for 30%CuPS, which were assigned to metallic Cu^{0}/Cu^{+} species suggesting that Cu^{2+} have been reduced to Cu^{0}/Cu^{+}. Nevertheless, the deconvoluted $Cu2p_{3/2}$ peak of reduced CuPS catalysts show small amount of Cu^{2+} at binding energy around 935.7-936.3 eV, which existed on the catalyst samples because they have been ex-situ reduced prior to measure by XPS. The appearance of Cu^{+} species on reduced CuPS catalysts exhibited the strong interaction between Cu and phyllosilicate structure [32].

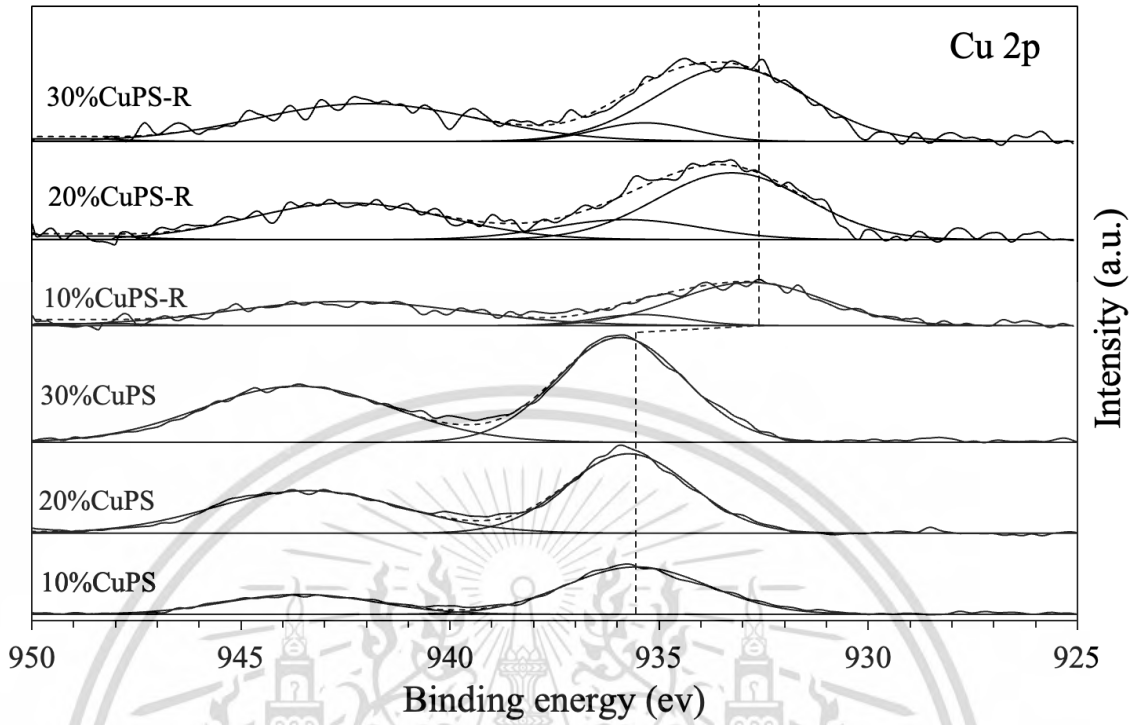

Figure 4.10 XPS spectra of Cu 2p of CuPS catalysts after calcination and reduction CuPS catalysts.

4.1.8. NH_3-Temperature program desorption (NH_3-TPD)

The acidity and acid strength of all CuPS catalysts were investigated by NH_3-TPD, as the result illustrates in **Figure 4.11**. The main NH_3 desorption peak with the center around 110 °C was found on all calcined CuPS catalyst while for all reduced CuPS catalyst, this peak shift to higher temperature with the center around 130 °C. Normally, the acid strength can be classified as weak acid site (<120 °C) medium acid site (160 °C) and strong acid site (> 250 °C) [36]. Therefore, both calcined and reduced CuPS catalysts occupied mostly weak acid sites. However, all reduced CuPS catalyst exhibited stronger acid strength at 110 to 130 °C than calcined CuPS catalyst because the copper species can be exposed on the surface after reduction. These weak acid site on CuPS catalysts could be obtained from surface OH group and unsaturated/defective Si^{4+} and various Cu species [28,37]. In addition, all CuPS catalysts also show a minor peak at medium acid site.

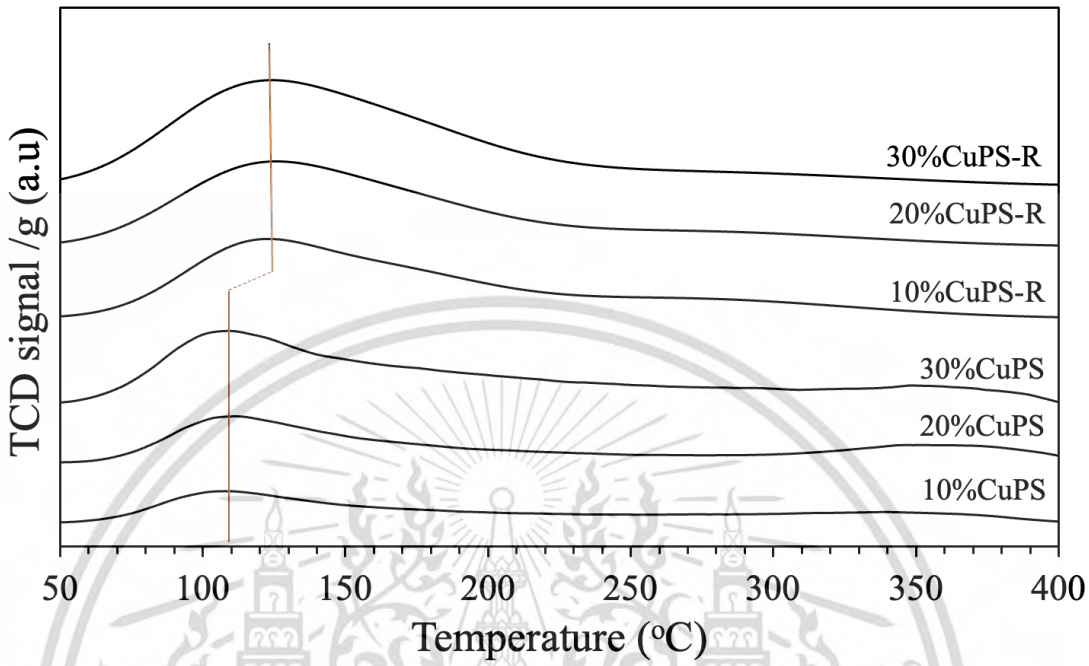

Figure 4.11 NH_3 TPD of CuPS catalysts

The total acidity calculated from the deconvoluted peak by the Gaussian deconvolution method and Lewis and Brønsted acid determined by Py-IR were summarized in **Table 4.3.** There were 277.0, 353.2, and 444.3 μmol/g for calcined 10%CuPS, 20%CuPS, and 30%CuPS, respectively. It can be noted that increasing of acidity on calcined CuPS catalysts were in line with the amount of copper loading. For CuPS-R, total acidity were 441.9, 474.2, and 520.9 μmol/g for 10%CuPS-R, 20%CuPS-R, and 30%CuPS-R, respectively. According to total acidity, the reduced CuPS catalysts have higher NH_3 adsorption than calcined CuPS catalysts. During reduction the phyllosilicate structure was destroyed resulting to copper exposed into the surface. It more opportunity to adsorb by NH_3 [38].

Table 4.3 Acidity of all CuPS catalysts

catalyst	Acidity (μmol)						
	Weak [a]	Medium[a]	Strong [a]	Total acidity[a]	Lewis's a[b]	Brønsted[b]	L/B[b]
10%CuPS	67.3	130.8	78.9	277.0	-	-	-
20%CuPS	104.3	166.5	82.7	353.2	-	-	-
30%CuPS	126.9	229.8	87.5	444.3	189.9	36.3	5.2
10%CuPS-R	186.0	227.5	28.4	441.9	-	-	-
20%CuPS-R	202.2	238.3	33.7	474.2	-	-	-
30%CuPS-R	237.5	283.5	40.8	520.9	270.8	44.8	6.0

[a] Determined by NH_3-TPD.

[b] Determined by Py-IR

4.1.9. Pyridine-adsorbed infrared spectroscopy (Py-IR)

Py-FTIR was used to quantitative analyze the Brønsted and Lewis acid sites of catalyst. As shown in **Figure 4.12**, the Brønsted acid site shows peak at 1530 and 1633 cm^{-1} of hydroxyl groups (such as SiO-H) of both catalysts. Adsorption bands at 1451.2 and 1609.8 cm^{-1} were pyridine-adsorbed Lewis's acid sites could attributed Cu^{2+} species of 30%CuPS, while adsorption band at 1448.7 and 1607.3 cm^{-1} were pyridine-adsorbed Lewis's acid sites could attributed Cu^{+} species of Cu–O–SiO_x interface of reduced CuPS [17,39]. The Lewis acid strength can be seen by higher wavenumber. So, 30%CuPS shows the stronger Lewis acid site. The Lewis acid as show in **Table 4.3** were 189.9 and 270.8 μmol/g for 30%CuPS and 30%CuPS-R respectively. The Brønsted were 36.3 and 44.8 for

for 30%CuPS and 30%CuPS-R respectively. Ratio of L/B follows the order: CuPS-R (6.0) > CuPS (5.2). Brønsted and Lewis acid sites control different reactions; therefore, an appropriate L/B ratio is extremely important for catalytic transfer hydrogenation.

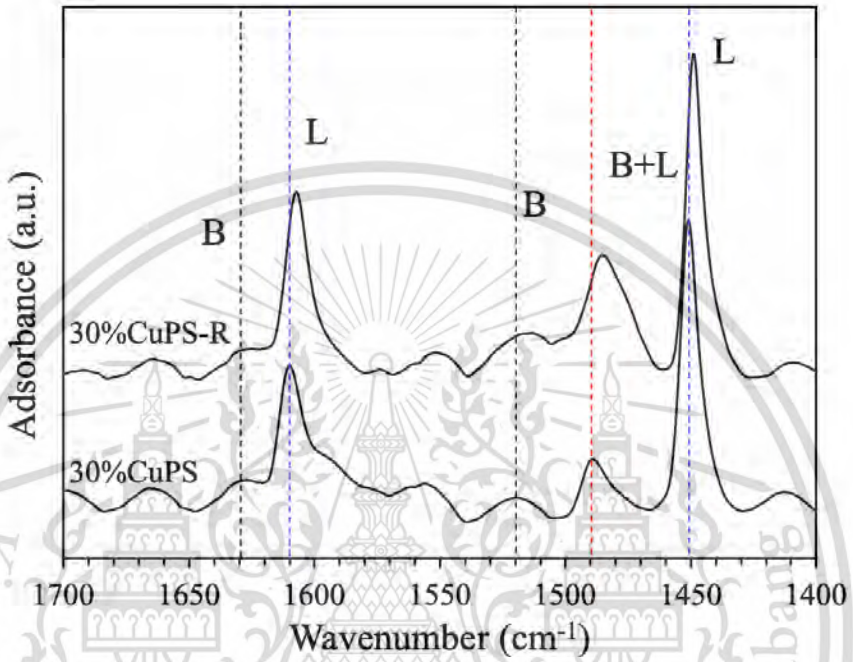

Figure 4.12. Pyridine-adsorbed IR spectra of 30%CuPS

4.2 Catalytic activity of CuPS of CuPS catalysts in liquid phase catalytic transfer hydrogenation of furfural to GVL

To understand the catalytic behavior of CuPS catalysts in the liquid phase selective hydrogenation of furfural (FF) to GVL. The effect of copper loading (10-30%CuPS) and type of copper species (Cu^0/CuO) have been verified. The reaction was carried out in 100ml of batch type stainless steel autoclave reactor at 160 °C using 2-propanol as a hydrogen donor. **Table 4.4** summaries the catalytic performance of CuPS catalysts with different copper loading and copper species in the liquid phase selective hydrogenation of furfural to GVL. The FF conversion for CuPS-R catalysts (in **Table 4.4,** entry 1-3) were 24%, 100% and, 100% for 10%CuPS, 20%CuPS and, 30%CuPS respectively. The completed conversion of FF can be obtained from the 20%CuPS and 30%CuPS catalysts. Although, the reduced catalysts gave higher conversion than calcined catalysts, the selectivity to GVL product was quite low (2-22%). The main product for reduced catalysts was furfuryl alcohol (FA). Because of the main active species of copper in reduced CuPS catalysts were metallic Cu^0 which usually acts as the active site for dehydrogenation of 2-propanol. Moreover, the existing of electrophilic Cu^+ species act as Lewis's acid site to activate C=O group in furfural shows the synergistic effect of $Cu^0$and Cu^+ resulting to high activity in the reduced catalysts [40].

On the other hand, the calcined CuPS catalysts, the conversion of furfural were 7% ,16% and, 14% for 10%CuPS, 20%CuPS and, 30%CuPS respectively. Although the calcined CuPS catalysts exhibited low catalytic conversion of FF (<20%), Isopropyl levulinate (IPL) and GVL were found as two main products. This could attribute to the existent of well-defined Cu^{2+} species by in situ TR-XANES and XPS, prefer to occur the hydrogenation pathway to produce IPL and GVL. Moreover, an increasing of copper loading on calcined catalysts shows ascending order with GVL selectivity. The maximum GVL selectivity at 37% can obtained from 30%CuPS catalyst. FA was not found in calcined

CuPS, which is interesting. It could suggest that Cu^{2+} species on calcined CuPS is effective at transforming FA to GVL. From Py-IR, 30%CuPS shows the stronger Lewis acid so it can stronger the FF adsorption. However, at a certain Lewis acid strength, the adsorption of FA (the product) becomes so strong that it might block the catalyst surface sites, resulting in decreased conversion but increased selectivity to GVL [41].

Table 4.4 The catalytic performance of CuPS catalysts in liquid phase catalytic transfer hydrogenation of furfural to GVL [a]

Entry	Catalysts	Conversion (%)	Selectivity (%)				Yield (%)
			FA	GVL	IPL	LA	GVL
1	10%CuPS-R	24	84	2	2	12	0
2	20%CuPS-R	100	88	12	0	0	12
3	30%CuPS-R	100	75	22	0	3	22
4	10%CuPS	7	0	17	83	0	1
5	20%CuPS	16	0	26	74	0	4
6	30%CuPS	14	0	37	42	21	5

[a] reaction conditions: furfural 200 µL (2.4 mmol), Isopropanol 10 mL, N_2 10 bar ,160°C, 2h.

To confirm the effectiveness of calcined CuPS. **Figure 4.13** shows the results of a study on catalytic performance using FA as a substrate. 30%CuPS shows the highest conversion of furfuryl alcohol (98.8%) with a high yield of GVL (53.8%). Which suggesting that FA favor esterification with 2-propanol via stronger Lewis's acid site. While 30%CuPS-R shows the lower conversion (31.8%) than 30%CuPS. Therefore, calcined is suitable for FA, this is possibly due to the metal oxide's role for transformation of FA to the next step.

From previous report, it can be seen that the step transfer hydrogenation was using metallic Cu^0 species. For the further step from FA to GVL was used Cu^{2+} species. The bi-

functional catalyst of hydrogenation site (metallic Cu^0) and acid site (Cu^{2+}) could be study in the next part.

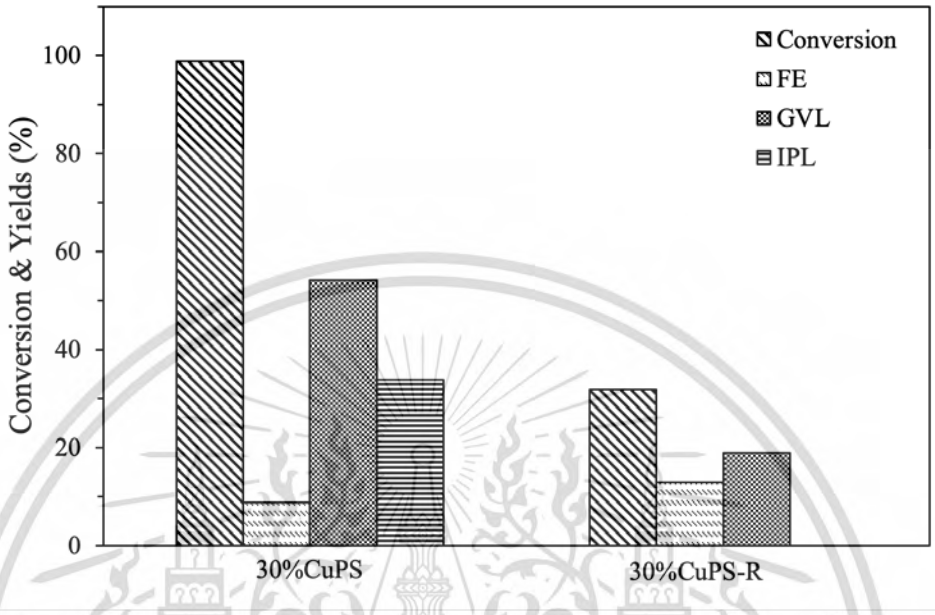

Figure 4.13 Catalytic performance of 30%CuPS for liquid phase selective hydrogenation of furfuryl alcohol to GVL via CTH reaction. Reaction conditions: furfuryl alcohol 200 µL (2.4 mmol), Isopropanol 10 mL, N_2 10 bar ,160°C, 2h.

Part 2

Effect of physical mixing between 30%CuPS-R and 30%CuPS catalysts with various % ratios.

In this part, the combination between both type of catalysts has never been studied in liquid phase selective hydrogenation of furfural to GVL. To tune the acidity and acid strength of CuPS catalysts to achieve high catalytic performance in this reaction, the physical mixing of 30%CuPS-R and 30%CuPS with different %wt. ratios (30:70, 50:50 and, 70:30) have been investigated. The catalytic performance of all catalysts was evaluated in liquid phase catalytic transfer hydrogenation using 2-propanol as hydrogen donor. Furthermore, the effect of rection with time profile was studied.

4.3 Characterization of catalysts

In this section, the characterization of all physical mixing of of 30%CuPS-R and 30%CuPS with different %wt. ratios (30:70, 50:50 and, 70:30) catalysts were investigated as following:

4.3.1 NH_3-Temperature program desorption (NH_3-TPD)

The acidity and acid strength of physical mixing between 30%CuPS-R and 30%CuPS catalysts with various % wt. ratios were investigated by NH_3-TPD, as the result illustrates in **Figure 4.14**. The main NH_3 desorption peak with the center around 140 °C and 200 °C. The total acidity was 509.6, 498.2, and 464.1 μmol/g of 30%CuPS-R: 30%CuPS (%wt. ratio) (70:30), (50:50), and (30:70) respectively.

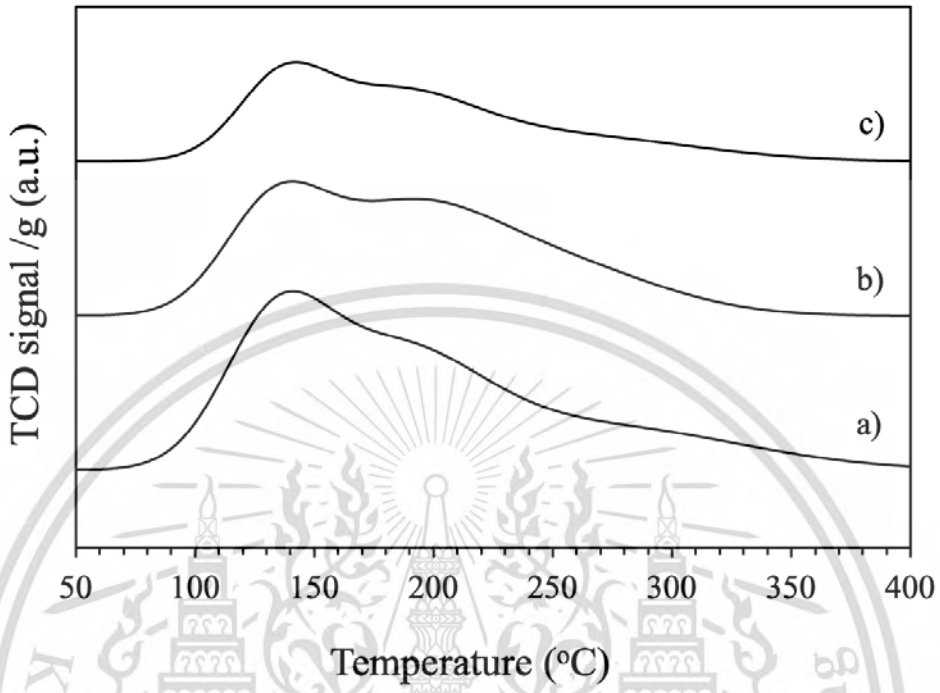

Figure 4.14 NH_3 TPD of physical mixing a) 70: 30 b) 50:50 and c) 30:70 of 30%CuPS-R: 30%CuPS (%wt. ratio)

Table 4.5 Acidity of physical mixing between 30%CuPS-R and 30%CuPS catalysts with various % wt. ratios.

30%CuPS-R: 30%CuPS (%wt. ratio)	Acidity (μmol)						
	Weak [a]	Medium[a]	Strong [a]	Total acidity[a]	Lewis's a[b]	Brønsted[b]	L/B[b]
70: 30	186.0	263.1	60.5	509.6	249.3	42.1	5.9
50:50	179.9	245.2	73.1	498.2	223.6	39.1	5.7
30:70	152.1	234.6	77.4	464.1	204.4	37.0	5.5

[a]Determined by NH_3-TPD. [b]Determined by Py-IR

4.3.2. Pyridine-adsorbed infrared spectroscopy (Py-IR)

Figure 4.15 shows Py-FTR of physical mixing between 30%CuPS-R and 30%CuPS catalysts with various % wt. ratios**,** the Brønsted acid site showed peak at 1530 and 1633 cm^{-1} of hydroxyl groups (such as SiO-H) of both catalysts. Adsorption bands at 1450 and 1609 cm^{-1} were pyridine-adsorbed Lewis's acid sites could attribute Cu^{2+} species of calcined or Cu^{+} species of Cu–O–SiO_x interface of reduced CuPS. The peak at 1487 cm^{-1} is combination effect of Brønsted+Lewis acid site. The acidity listed in **Table 4.5**. The Lewis acid were 249.3, 223.6, and 270.8 μmol/g of 30%CuPS-R: 30%CuPS (%wt. ratio) (70:30), (50:50), and (30:70) respectively. The Brønsted were 42.1, 39.1, and 37.0 of 30%CuPS-R: 30%CuPS (%wt. ratio) (70:30), (50:50), and (30:70) respectively. Ratio of L/B follows the order: 70:30 (5.9) >50:50 (5.7) > 30:70 (5.5).

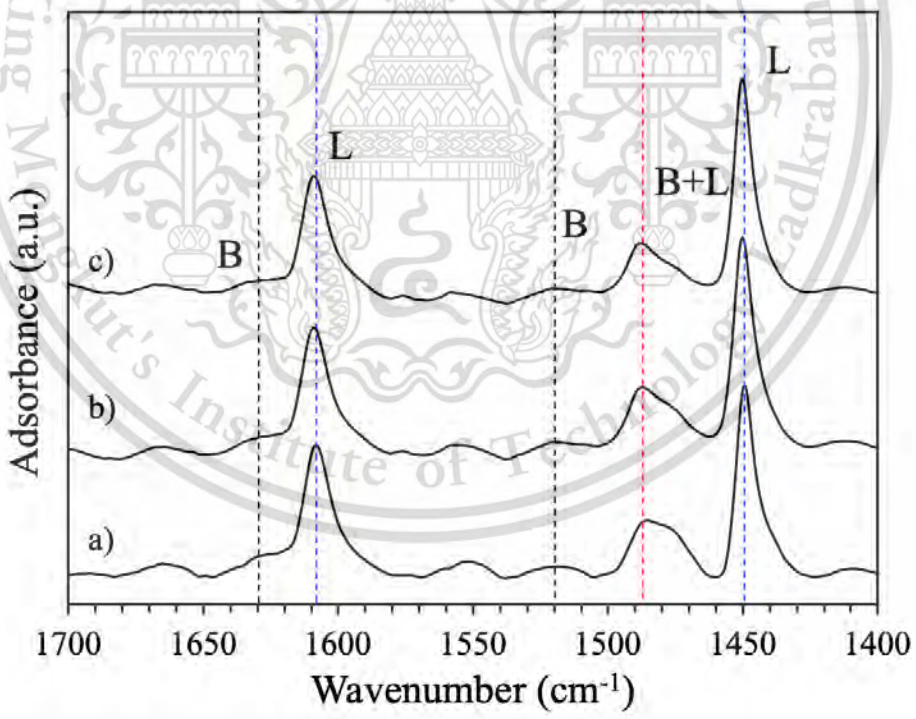

Figure 4.15. Pyridine-adsorbed IR spectra of physical mixing catalysts mixing a) 70: 30 b) 50:50 and c) 30:70 of 30%CuPS-R: 30%CuPS (%wt. ratio)

4.4 Catalytic activity of physical mixing catalysts in liquid phase catalytic transfer hydrogenation of furfural to GVL

The physical mixing between 30%CuPS-R and 30%CuPS with different %wt. ratios (30:70, 50:50 and, 70:30) has been performed in this reaction. **Table 4.6** summaries the catalytic performance of physical mixing CuPS catalysts in liquid phase selective hydrogenation of furfural to GVL at 160 °C. The conversion of furfural at 2 h was increased from 48-100% when increased amount of 30%CuPS-R from 30-70%. The completed conversion can be obtained from physical mixing ratio 50:50 and 70:30. This could attribute to metallic Cu^0 that enough to convert total amount of FF was 50% wt. Furthermore, the maximum GVL selectivity at 56% was observed on physical mixing ratio 50:50 while other ratios show lower GVL selectivity. It can be concluded that the suitable physical mixing ratio of CuPS catalyst was 50:50 because it can be reached the maximum GVL selectivity (56%) as well as the FF conversion (100%). According to these results, both metallic Cu^0 and Cu^{2+} species is the important active species in liquid phase selective hydrogenation of FF to GVL. It can be observed that catalyst consisted of more metallic Cu^0 species than Cu^{2+} species will promote FA production. On the other hand, catalysts consisted of more Cu^{2+} species can accelerate the further steps from FA to GVL product as shows in **Figure 4.16**. When increased Cu^{2+} species in physical mixing the rearrangement selectivity (FE, IPL, LA and GVL) was increased.

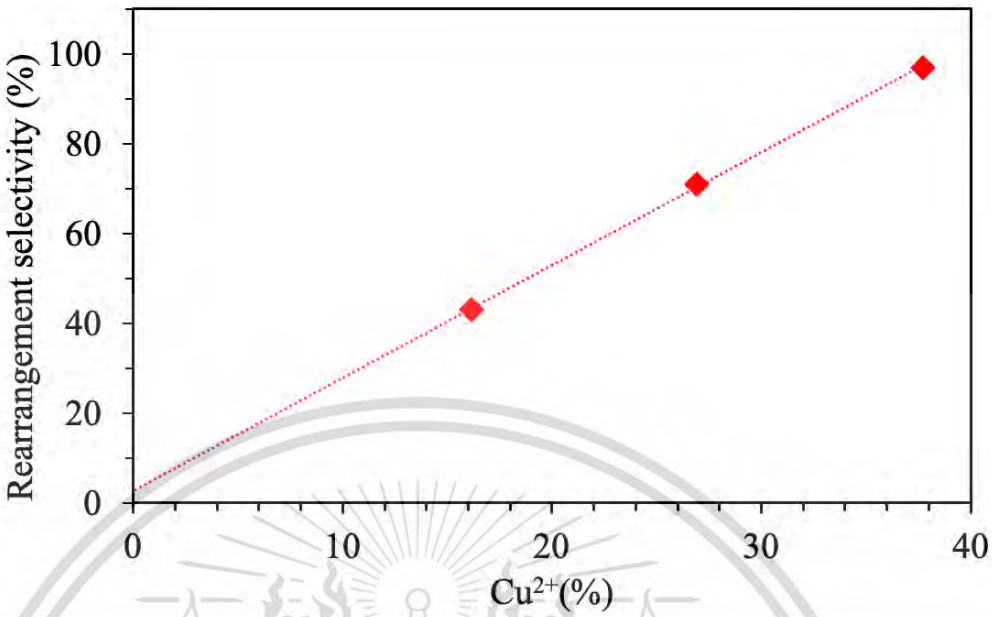

Figure 4.16 The relationship between Cu^{2+} species vs rearrangement selectivity

Table 4.6 The catalytic performance of physical mixing between 30%CuPS-R and 30%CuPS catalysts with various % wt. ratios in liquid phase selective hydrogenation of furfural to GVL[a].

Entry	30%CuPS-R: 30%CuPS (%wt. ratio) [b]	Cu^0	Cu^{2+}	Conversion (%)	Selectivity (%)					Yield (%)
					FA	GVL	IPL	LA	FE	GVL
1	70: 30	64.2	16.2	100	50	43	0	0	7	43
2	50:50	45.9	26.9	100	8	56	15	0	21	56
3	30:70	27.5	37.7	48	4	40	44	13	0	19

[a] reaction condition: reaction conditions: furfural 200 µL (2.4 mmol), Isopropanol 10 mL, N_2 10 bar ,160°C, 2h.

[b] based on total catalyst 200 mg.

The physical mixing ratio 50:50 was studied further as a catalyst on the production of GVL from furfural. **Figure 4.17** shows the change in product distribution with reaction time from 30- 480 min. According to these results, at 30 min of the reaction, the furfural conversion was low (36.4%) and FA was observed as the major product (66.5%). The furfural conversion was complete (100%) at time from 120 min, FA was decreased while the GVL increased. It can be suggested that FA is primary product to produced GVL. The IPL and FE exhibit approximately 20% and decrease with time. With increasing the time from 120 to 480 min, the GVL was increased from 12% to 86%. The optimum reaction time to obtain high GVL selectivity is 480 min. The reaction time analysis suggests that the CTH of furfural to GVL occurs thorough FA,FE, and IPL intermediates[25].

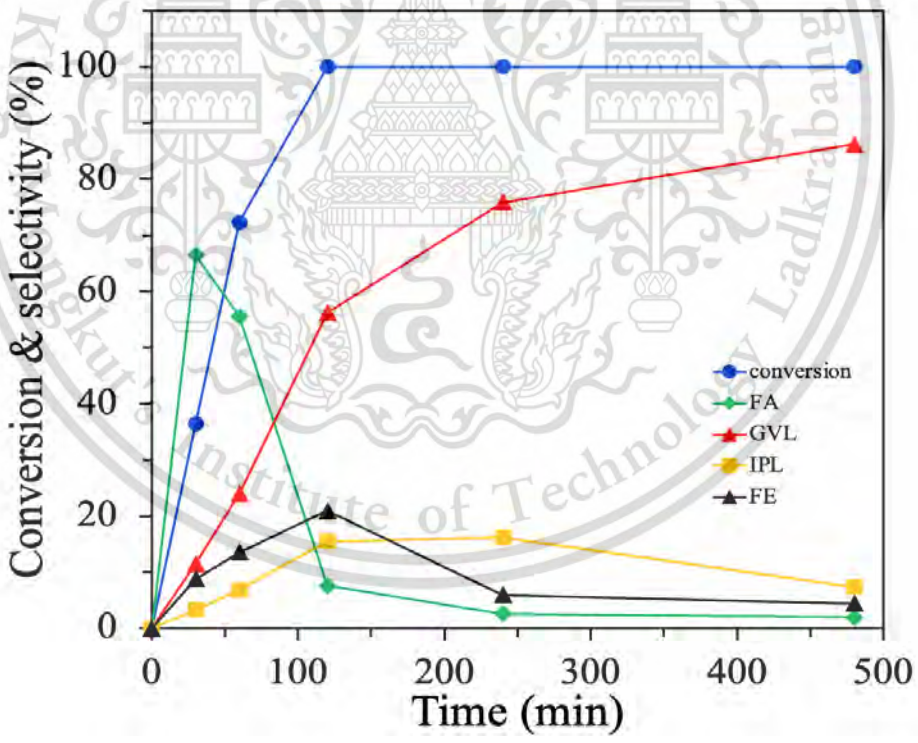

Figure 4.17 Effect of time on reaction over physical mixing (50:50) catalyst.

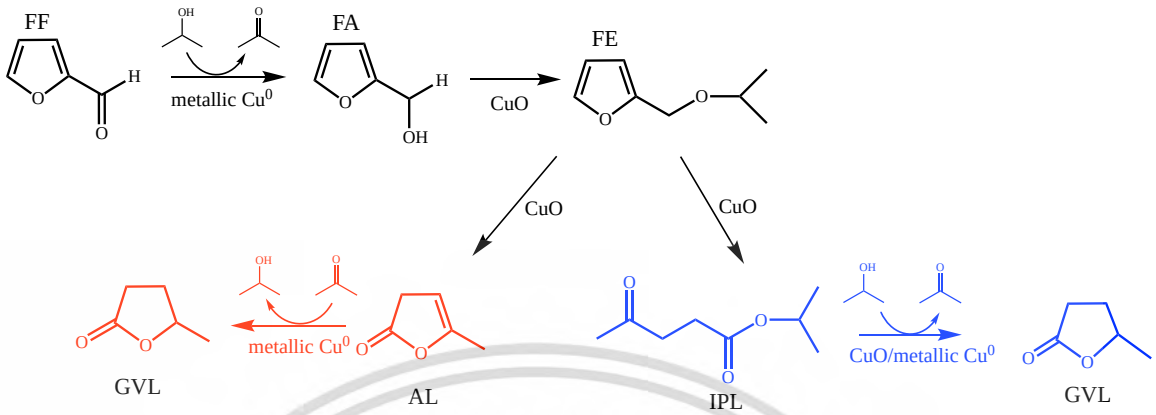

Figure 4.18 Reaction pathway of furfural to GVL.

The one-pot conversion of FF to GVL is illustrated in the reaction network proposed in **Figure 4.18**. It can be seen that FF can be convert to FA by metallic Cu^0. metallic Cu^0 promoted furfural Meerwein-Ponndorf-Verley (MPV) reduction into furfuryl alcohol (FA). Then, furfuryl alcohol reacts with 2-propanol, which used as a solvent, resulting in furfuryl ether (FE) was form and FE was rearrangement AL or FE can ring-opening reaction to form IL intermediated using CuO species. The hydrogenation of the C=C bond to GVL by using metallic Cu^0 [42]. While IPL transform to GVL by cyclization and hydrogenation reaction using CuO and metallic Cu^0 respectively [43,44].

Part 3

Effect of secondary metal doping over CuPS catalyst (1%Mn_2O_3/CuPS and 1%ZnO/CuPS)

The secondary metal catalysts were prepared by impregnation method. After that the characteristic of 1%Mn_2O_3/CuPS and 1%ZnO/CuPS are demonstrated in this section 4.5. The result of catalytic performances in the catalytic transfer hydrogenation of furfural to furfuryl alcohol are shown in section 4.6.

4.5 Characterization of catalysts

4.5.1 Physiochemical properties of CuPS catalysts.

Table 4.7 The physical properties of secondary metal over CuPS catalysts

Catalysts	Metal[a] (%wt.)		N_2-adsorption desorption		
	Cu	M[b]	S_{BET} (m^2/g)	Pore volume (cm^3/g)	Pore size dimeter (nm)
30%CuPS-R	30.8	-	425	5.4	5.1
1%Mn_2O_3/CuPS	30.8	1.0	196	4.1	8.4
1%ZnO/CuPS	30.8	1.1	176	3.0	6.8

[a] determined by XRF

[b] M is second metals (Mn and Zn)

Table 4.7 summarized the amount of metal loading, BET surface area, pore volume, and average pore size diameter of catalysts. The actual amount of Cu on 30%CuPS catalysts determined by XRF was 30.8 wt.% which consisted with the desired amount of Cu loading on catalysts. Moreover, the second metals loading such as Mn and Zn were

found to be 1.0 and 1.1 wt.% on 1%Mn_2O_3/CuPS and 1%ZnO/CuPS, respectively. The BET surface area of 30%CuPS-R was 425 m^2/g. When the secondary metals (Mn_2O_3 and ZnO) impregnated on 30%CuPS-R, the BET surface area dramatically decreased from 425 to 196 and 176 m^2/g for 1%Mn_2O_3/CuPS and 1%ZnO/CuPS, respectively. Moreover, the pore volume of both bimetallic catalysts trends to decrease indicating that Mn_2O_3 and ZnO was adsorbed in the pore size of 30%CuPS-R catalyst

4.5.2 X-ray diffraction pattern, XRD

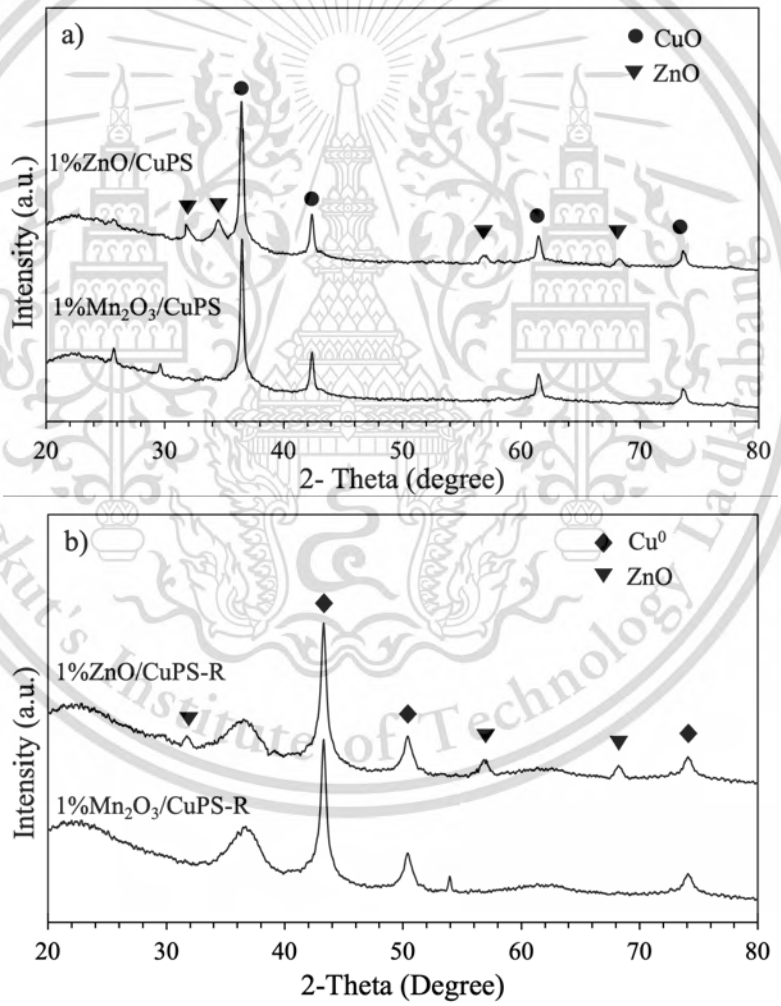

Figure 4.19 XRD pattern of 30%CuPS, 1%Mn_2O_3/CuPS, and 1%ZnO/CuPS catalysts after a) calcination at 400 °C, b) reduction at 250 °C.

The XRD pattern of 30%CuPS, 1%Mn_2O_3/CuPS, and 1%ZnO/CuPS catalysts after calcined at 400 °C and reduced at 250 ° show in **Figure 4.19**. According to calcined catalysts (**Figure 4.19 a**), The diffraction peaks of ZnO at 2θ = 31.7°, 34.4°, 56.5°, and 68.1° were observed on 1%ZnO/CuPS. In contrast with 1%Mn2O3/CuPS was not observed the diffraction pattern of MnOx resulting was not clarify the species of MnOx. It will clarify by XPS technique. Both catalysts also exhibited the diffraction peaks at 2θ = 36.4°, 42.5°, 61.6°, and 73.5° which were corresponded to CuO species. For reduced catalysts (**Figure 4.19 b**), the diffraction peaks of metallic Cu^0 at 2θ = 43.2°, 50.6°, and 74.3° were strongly observed on 1%Mn_2O_3/CuPS-R and 1%ZnO/CuPS-R catalysts.[45] The characteristic peak of ZnO were existed on reduced 1%ZnO/CuPS-R.

4.5.3 NH_3-Temperature program desorption (NH_3-TPD)

The acidity and acid strength of catalysts were investigated by NH_3-TPD, as the results illustrate in **Figure 4.20.** According to NH_3-TPD profiles of calcined catalysts, two main desorption peaks around 170°C and 340 °C were found on 1%Mn_2O_3/CuPS and 1%ZnO/CuPS. After reduction, two main desorption peaks were significantly shifted to lower temperature suggesting to the presence of weak acid site on reduced catalysts. The amount of total acidity calculated from the deconvoluted peak compared with 1%NH_3 in He of catalysts were reported in **Table 4.8.** The total acidity of calcined catalysts was 593.1 and 605.3 μmol/g for 1%Mn_2O_3/CuPS and 1%ZnO/CuPS respectively. For reduced catalysts, the total acidity was slightly increased to 610.8 and 623.6 μmol/g for 1%Mn_2O_3/CuPS-R and 1%ZnO/CuPS-R respectively. It was found that reduced catalysts had a higher acidity than calcined catalysts since the layer of phyllosilicate structure was destroyed during reduction resulting to decrease the coordinate unsaturated Si^{4+} and surface silanol group were decreased.

Table 4.8 Acidity of secondary metal doping over CuPS catalysts calculated from NH_3-TPD

Catalysts	Acidity (μmol)			
	Weak	Medium	Strong	Total acidity
1%Mn_2O_3/CuPS	96.3	426.6	70.2	593.1
1%ZnO/CuPS	127.1	393.1	85.1	605.3
1%Mn_2O_3/CuPS-R	211.5	366.9	32.4	610.8
1%ZnO/CuPS-R	240.5	336.9	25.9	623.6

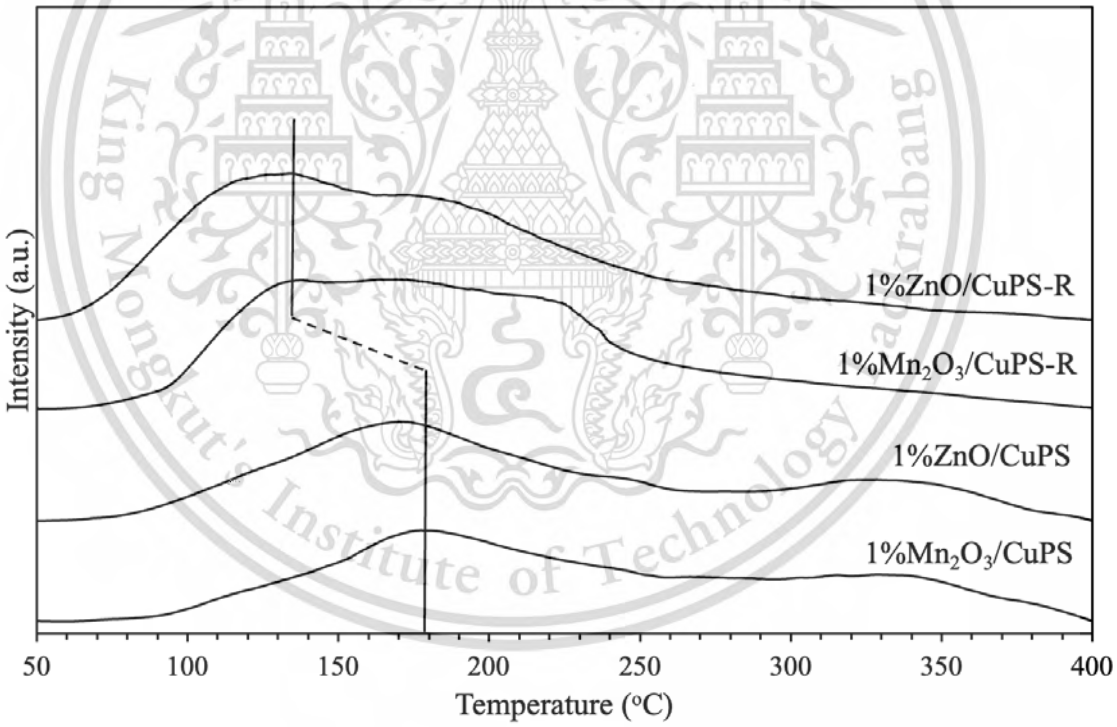

Figure 4.20 NH_3-TPD of secondary metal over CuPS catalysts.

4.5.4. X-ray Photoelectron Spectroscopy (XPS)

The chemical composition and electronic states of catalysts were identified by XPS as the results illustrated in **Figure 4.21.** According to Cu $2p_{3/2}$ spectra, the peak at binding energy around 935.4-925.6 eV which assigned to Cu^{2+} species were found on calcined catalysts 1%Mn_2O_3/CuPS, and 1%ZnO/CuPS[46]. Furthermore, the peak of Mn 2p and Zn 2p as shown in **Figure 4.22 a.** The peak of Mn 2p at binding energy around 640.9 eV with a satellite peak at 648.5 eV was clearly observed on 1%Mn_2O_3/CuPS indicating to the existence of Mn_2O_3.[47] Moreover, it can be observed the Zn 2p peak at binding energy around 1021.9 which attributed to Zn^{2+}on 1%ZnO/CuPS as shown in **Figure 4.22 b** [48].

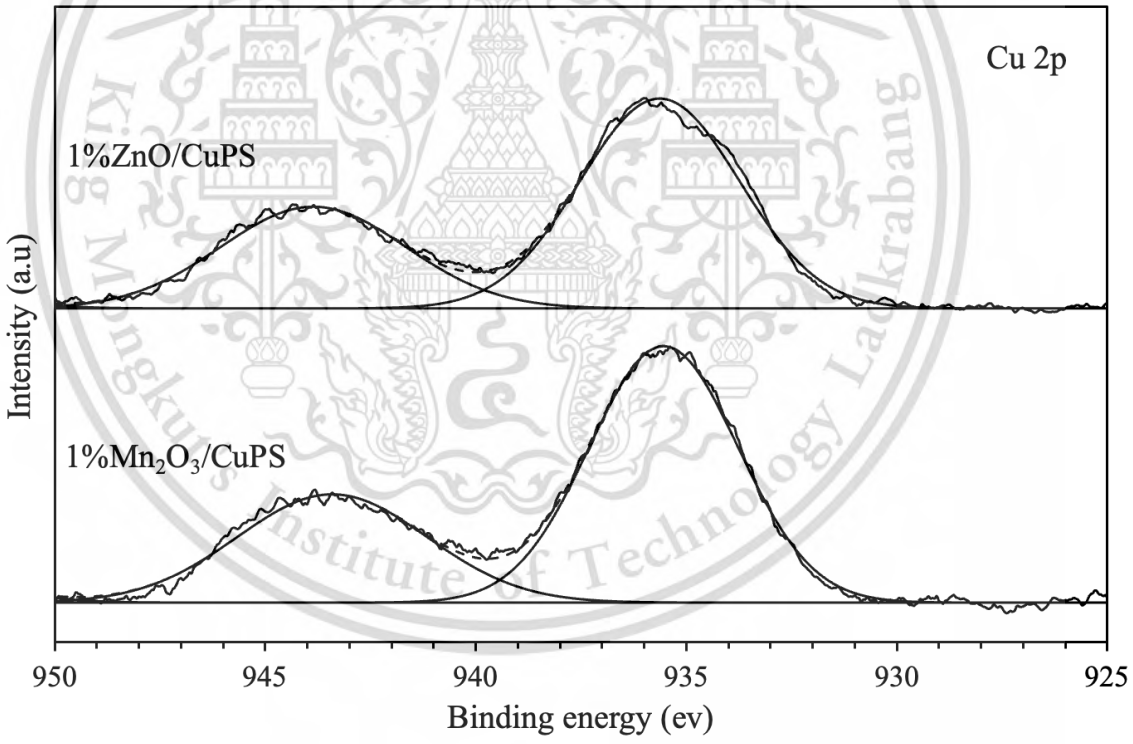

Figure 4.21 XPS spectra of Cu 2p for 1%Mn_2O_3/CuPS and 1%ZnO/CuPS

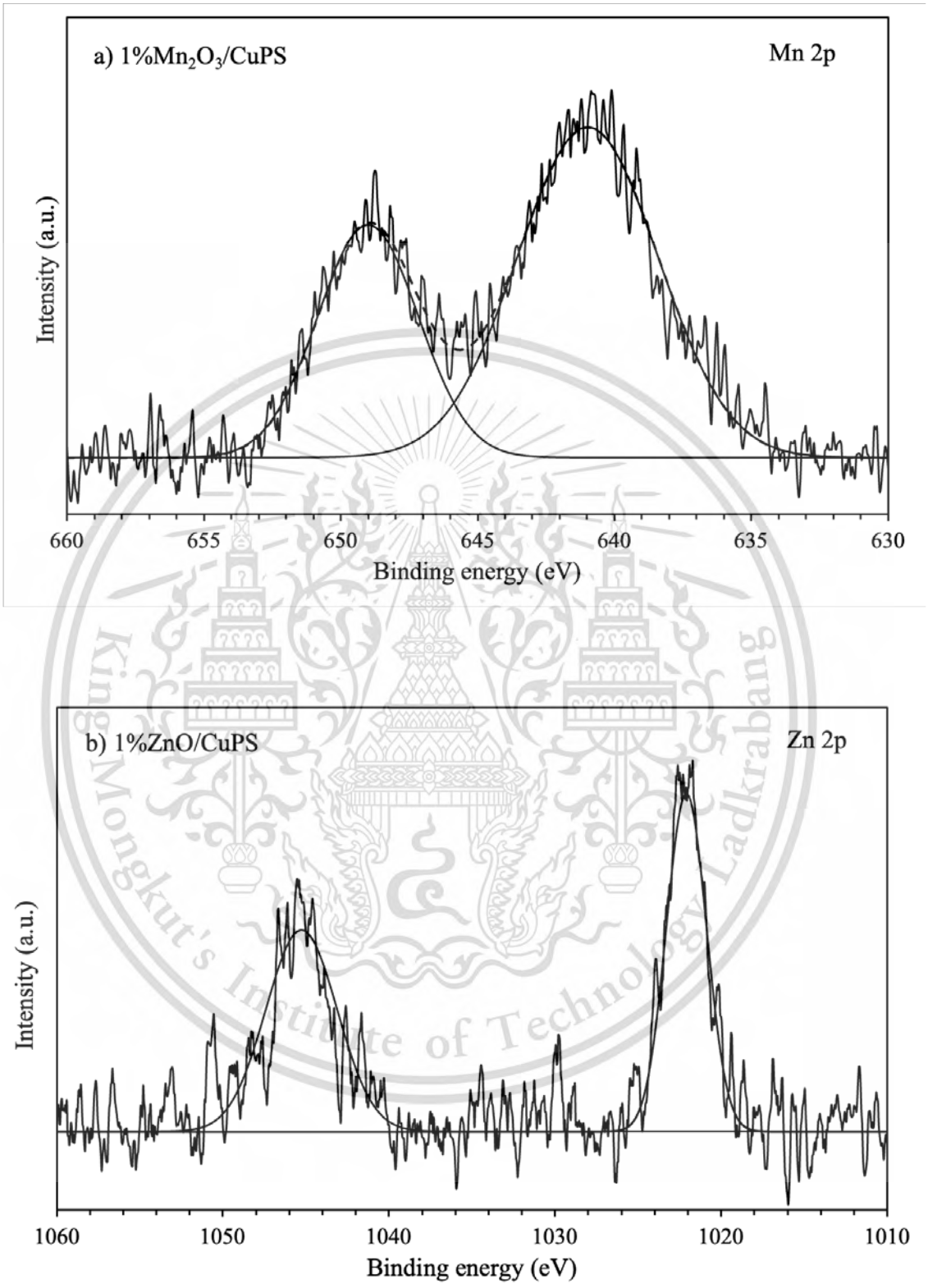

Figure 4.22 XPS spectra of catalysts; a) Mn 2p for 1%Mn_2O_3/CuPS, and b) Zn 2p for and 1%ZnO/CuPS

4.6 Catalytic activity metal oxide promotors (Mn_2O_3, ZnO) on 30%CuPS catalysts in liquid phase catalytic transfer hydrogenation of furfural to GVL

To understand the catalytic performance of metal oxide promotors (Mn_2O_3, ZnO) on 30%CuPS catalysts, the catalytic transfer hydrogenation of furfural to furfuryl alcohol have been carried out in 100 ml of batch type stainless steel autoclave reactor at 160 °C using isopropanol as a hydrogen donor. **Table 4.9.** summaries the catalytic performance of catalysts in liquid-phase selective hydrogenation of furfural to GVL. According to results, the main products obtained from this reaction is furfuryl alcohol (FA), gamma-valerolactone (GVL), and isopropyl levulinate (IPL). In our case, the selectivity of furfuryl alcohol was 75%. For 1%Mn_2O_3/CuPS-R, the conversion of furfural was slightly decrease to 97% with high selectivity to FA at 97%, indicating that Mn_2O_3 can improve the selectivity of FA. On the contrary for 1%ZnO/CuPS-R, the conversion of furfural was dramatically decreased to 61% with 91% selectivity of FA. These indicated that ZnO inhibited the catalytic transfer hydrogenation of furfural. It might be because of ZnO reduce the BET surface area and enhance the total acidity of 1%ZnO/CuPS. Furthermore, the physical mixing catalysts between 30%CuPS-R and at 50:50 (wt.%) was performed, the complete furfural conversion (100%) with 96% of FA selectivity can obtain from physical mixing of 30%CuPS-R+1%Mn_2O_3/CuPS catalysts. It is indicated that the synergetic effect of Mn_2O_3 and Cu^0/Cu^+ on physical mixing catalyst of 30%CuPS-R+1%Mn_2O_3/CuPS promotes the catalytic transfer hydrogenation of furfural to furfuryl alcohol on both conversion and selectivity.[49] In addition, the physical mixing catalyst of 30%CuPS-R+1%ZnO/CuPS catalysts shows a high conversion of furfural at 99% with 93% selectivity to FA. It can be suggested that from the XRD pattern of 1%Mn_2O_3/CuPS or 1%ZnO/CuPS after calcination show the CuO species. From the literature[33]; the Cu^{2+} species in the CuO would virtually exist in 4-coordinate square planar geometry resulting in it cannot promoted GVL selectivity.

Table 4.9 The catalytic performance of secondary metal over CuPS catalysts in liquid-phase selective hydrogenation of furfural to furfuryl alcohol.[a]

Catalysts	Conversion (%)	Selectivity (%)		
		FA	GVL	IPL
1%Mn_2O_3/CuPS-R	97	97	3	0
1%ZnO/CuPS-R	61	91	9	0
30%CuPS-R+ 1%Mn_2O_3/CuPS	100	96	4	0
30%CuPS-R+1%ZnO/CuPS	99	93	7	0

[a] Reaction condition: Furfural 200 µL (2.4 mmol), isopropanol 10 ml (130.8 mmol), catalyst 200 mg, temperature 160°C, 2 h, N_2 pressure 10 bar.

CHAPTER 5
CONCLUSION AND DISCUSSION

5.1 Conclusions

In this thesis, the study on the conversion of furfural to GVL over CuPS catalysts were investigated. The effect of copper loading and Cu species (Cu^0, CuO), effect of physical mixing between 30%CuPS-R and 30%CuPS catalysts with various % wt. ratios and effect of secondary metal were investigated.

The CuPS was successfully synthesized by ammonia evaporation hydrothermal method. The copper loading from 10-30% give the higher surface area due to the more formation of octahedral layered structure. The 30%CuPS is a good candidate for catalytic transfer hydrogenation of furfural to GVL. The 30%CuPS-R gives a complete furfural conversion (100%) whereas 30%CuPS gives a highest GVL selectivity. The metallic Cu0 species on reduced CuPS catalyst act as active species for hydrogenation of furfural to furfuryl alcohol while CuO species on calcined CuPS catalyst play an important role to convert furfuryl alcohol to GVL

From the physical mixing, the various physical mixing ratio between 30%CuPS-R and 30%CuPS to adjust the ratio of metallic Cu^0/CuO effect to conversion of furfural and selectivity of GVL. The 30%CuPS-R and 30%CuPS at (50:50) shows the best catalytic performance in liquid phase hydrogenation of furfural to GVL (100% of furfural conversion with 86% of GVL selectivity).

1%ZnO/CuPS and 1%Mn_2O_3/CuPS could not improve catalytic performance in liquid phase hydrogenation of furfural to GVL because adding of ZnO and Mn_2O_3 on 30%CuPS increase the copper particle size affect to decrease the active species. Both 1%ZnO/CuPS and 1%Mn_2O_3/CuPS catalysts exhibited lower catalytic activity than reduced 30%CuPS catalyst. However, 1%Mn_2O_3/CuPS can promote the catalytic transfer

hydrogenation of furfural to furfuryl alcohol (97% conversion of furfural, 97% selectivity to FA).

5.2 Suggestions

5. 2. 1 Secondary alcohol (2-butanol, 2-pentanol, etc.) should be study the H-donor for catalytic transfer hydrogenation.

5. 2. 2 Reusability could by study in liquid phase catalytic transfer hydrogenation of furfural

References

[1] E.L. Kunkes, D.A. Simonetti, R.M. West, J.C. Serrano-Ruiz, C.A. Gärtner, J.A. Dumesic. 2008. Catalytic Conversion of Biomass to Monofunctional Hydrocarbons and Targeted Liquid-Fuel Classes, Science. 322: 417–421.

[2] G.W. Huber, S. Iborra, A. Corma. 2006. Synthesis of Transportation Fuels from Biomass: Chemistry. Catalysts, and Engineering, Chem. Rev. 106: 4044–4098.

[3] X. Li, P. Jia, T. Wang. 2016. Furfural: A Promising Platform Compound for Sustainable Production of C_4 and C_5 Chemicals, ACS Catal. 6: 7621–7640.

[4] D.M. Alonso, S.G. Wettstein, J.A. Dumesic. 2013. Gamma-valerolactone, a sustainable platform molecule derived from lignocellulosic biomass, Green Chem. 15 :584.

[5] J. Long, W. Zhao, H. Li, S. Yang. 2020. Furfural as a renewable chemical platform for furfuryl alcohol production, in: Biomass, Biofuels, Biochemicals, Elsevier: pp. 299–322.

[6] H.P. Winoto, B.S. Ahn, J. Jae. 2016. Production of γ-valerolactone from furfural by a single-step process using Sn-Al-Beta zeolites: Optimizing the catalyst acid properties and process conditions, Journal of Industrial and Engineering Chemistry. 40: 62–71.

[7] S. Zhu, Y. Xue, J. Guo, Y. Cen, J. Wang, W. Fan. 2016. Integrated Conversion of Hemicellulose and Furfural into γ-Valerolactone over Au/ZrO_2 Catalyst Combined with ZSM-5, ACS Catal. 6: 2035–2042.

[8] L. Bui, H. Luo, W.R. Gunther, Y. Román-Leshkov. 2013. Domino Reaction Catalyzed by Zeolites with Brønsted and Lewis Acid Sites for the Production of γ-Valerolactone from Furfural, Angew. Chem. Int. Ed. 52: 8022–8025.

[9] F. Dong, Y. Zhu, H. Zhao, Z. Tang. 2017. Ratio-controlled synthesis of phyllosilicate-like materials as precursors for highly efficient catalysis of the formyl group, Catal. Sci. Technol. 7: 1880–1891.

[10] P. Khemthong, C. Yimsukanan, T. Narkkun, A. Srifa, T. Witoon, S. Pongchaiphol, S. Kiatphuengporn, K. Faungnawakij. 2021.Advances in catalytic production of value-added biochemicals and biofuels via furfural platform derived lignocellulosic biomass, Biomass and Bioenergy. 148: 106033.

[11] P. Weerachawanasak, P. Krawmanee, W. Inkamhaeng, F.J. Cadete Santos Aires, T. Sooknoi, J. Panpranot. 2021. Development of bimetallic Ni-Cu/SiO2 catalysts for liquid phase selective hydrogenation of furfural to furfuryl alcohol, Catalysis Communications. 149: 106221.

[12] V. Sánchez, P. Salagre, M.D. González, J. Llorca, Y. Casters. 2020. Effect of the formation of NiCu alloy and use of biomass-derived furfural on the catalytic hydrogenation of furfural to THFA, Molecular Catalysis. 490: 110956.

[13] Y. Nakagawa, H. Nakazawa, H. Watanabe, K. Tomishige. 2012. Total Hydrogenation of Furfural over a Silica-Supported Nickel Catalyst Prepared by the Reduction of a Nickel Nitrate Precursor, ChemCatChem. 4: 1791–1797.

[14] W. Tolek, K. Khruechao, B. Pongthawornsakun, O. Mekasuwandumrong, F.J. Cadete Santos Aires, P. Weerachawanasak, J. Panpranot. 2021. Flame spray-synthesized Pt-Co/TiO2 catalysts for the selective hydrogenation of furfural to furfuryl alcohol, Catalysis Communications. 149: 106246.

[15] Z. Wang, X. Wang, C. Zhang, M. Arai, L. Zhou, F. Zhao. 2021. Selective hydrogenation of furfural to furfuryl alcohol over Pd/TiH2 catalyst, Molecular Catalysis. 508: 111599.

[16] J. Ruiz, C. Jimenez-Sanchidrian. 2007. Heterogeneous Catalysis in the Meerwein-Ponndorf-Verley Reduction of Carbonyl Compounds, COC. 11: 1113–1125.

[17] Y.-J. Tsou, T.D. To, Y.-C. Chiang, J.-F. Lee, R. Kumar, P.-W. Chung, Y.-C. Lin. 2020. Hydrophobic Copper Catalysts Derived from Copper Phyllosilicates in the Hydrogenation of Levulinic Acid to γ-Valerolactone, ACS Appl. Mater. Interfaces. 12: 54851–54861.

[18] B.P. Pinto, A.L.L. Fortuna, C.P. Cardoso, C.J.A. Mota. 2017. Hydrogenation of Levulinic Acid (LA) to γ-Valerolactone (GVL) over Ni–Mo/C Catalysts and Water-Soluble Solvent Systems, Catal Lett. 147: 751–757.

[19] X. Liu, Z. Li. 2021. Efficient transfer hydrogenation of levulinic acid (LA) to γ-valerolactone (GVL) over Ni/NiO–MC (MC = mesoporous carbon), Sustainable Energy Fuels. 5: 3312–3320.

[20] P.A. Son, S. Nishimura, K. Ebitani. 2014 Production of γ-valerolactone from biomass-derived compounds using formic acid as a hydrogen source over supported metal catalysts in water solvent, RSC Adv. 4 :10525.

[21] H. Zhang, W. Yang, I.I. Roslan, S. Jaenicke, G.-K. Chuah. 2019 A combo Zr-HY and Al-HY zeolite catalysts for the one-pot cascade transformation of biomass-derived furfural to γ-valerolactone, Journal of Catalysis. 375: 56–67.

[22] T. Toupance, M. Kermarec, J.-F. Lambert, C. Louis. 2002. Conditions of Formation of Copper Phyllosilicates in Silica-Supported Copper Catalysts Prepared by Selective Adsorption, J. Phys. Chem. B. 106: 2277–2286.

[23] H. A., M. P., T. Heine, L. Guimares. 2002. Clay Mineral Nanotubes: Stability, Structure and Properties, in: A. Innocenti (Ed.), Stoichiometry and Materials Science - When Numbers Matter, InTech.

[24] S. Sitthisa, T. Sooknoi, Y. Ma, P.B. Balbuena, D.E. Resasco. 2011. Kinetics and mechanism of hydrogenation of furfural on Cu/SiO2 catalysts, Journal of Catalysis. 277: 1–13.

[25] B. Srinivasa Rao, Yogita, D. Dhana Lakshmi, P.K. Kumari, N. Lingaiah. 2021. Influence of metal oxide and heteropoly tungstate location in mesoporous silica towards catalytic transfer hydrogenation of furfural to γ-valerolactone, Sustainable Energy Fuels. 5: 3719–3728.

[26] J. He, H. Li, Y. Xu, S. Yang. 2020. Dual acidic mesoporous KIT silicates enable one-pot production of γ-valerolactone from biomass derivatives via cascade reactions, Renewable Energy. 146: 359–370.

[27] J. Jiang, C. Tu, C. Chen, Y. Lin. 2018. Highly Selective Silica-supported Copper Catalysts Derived from Copper Phyllosilicates in the Hydrogenation of Adipic Acid to 1,6-hexanediol, ChemCatChem. 10: 5449–5458.

[28] F. Dong, G. Ding, H. Zheng, X. Xiang, L. Chen, Y. Zhu, Y. Li. 2016. Highly dispersed Cu nanoparticles as an efficient catalyst for the synthesis of the biofuel 2-methylfuran, Catal. Sci. Technol. 6: 767–779.

[29] C.J.G. Van Der Grift, A. Mulder, J.W. Geus. 1990. Characterization of silica-supported copper catalysts by means of temperature-programmed reduction, Applied Catalysis. 60. 181–192.

[30] A.J. Marchi, J.L.G. Fierro, J. Santamaría, A. Monzón. 1996. Dehydrogenation of isopropylic alcohol on a Cu/SiO_2 catalyst: a study of the activity evolution and reactivation of the catalyst, Applied Catalysis A: General. 142: 375–386.

[31] L. Huang, L. Lin, C.-C. Chen, R. Ye, L.-B. Zhu, J.-X. Yang, Y.-Y. Qin, J.-K. Cheng, Y.-G. Yao. 2022. β-Cyclodextrin promoted the formation of copper phyllosilicate on Cu-SiO2 microspheres catalysts to enhance the low-temperature hydrogenation of dimethyl oxalate, Journal of Catalysis. 413: 943–955.

[32] Z. Huang, F. Cui, J. Xue, J. Zuo, J. Chen, C. Xia. 2012. Cu/SiO_2 catalysts prepared by hom- and heterogeneous deposition–precipitation methods: Texture, structure, and catalytic performance in the hydrogenolysis of glycerol to 1,2-propanediol, Catalysis Today. 183: 42–51.

[33] C.J.G. Van Der Grift, P.A. Elberse, A. Mulder, J.W. Geus. 1990. Preparation of silica-supported copper catalysts by means of deposition-precipitation, Applied Catalysis. 59: 275–289.

[34] W. Prasanseang, K. Choojun, Y. Poo-arporn, A.-L. Huang, Y.-C. Lin, T. Sooknoi. 2022 Linear long-chain α-olefins from hydrodeoxygenation of methyl palmitate over copper phyllosilicate catalysts, Applied Catalysis A: General. 635: 118555.

[35] X. Li, J. Zhang, M. Zhang, W. Zhang, M. Zhang, H. Xie, Y. Wu, Y. Tan. 2019. The Support Effects on the Direct Conversion of Syngas to Higher Alcohol Synthesis over Copper-Based Catalysts, Catalysts. 9: 199.

[36] R.-P. Ye, L. Lin, J.-X. Yang, M.-L. Sun, F. Li, B. Li, Y.-G. Yao. 2017. A new low-cost and effective method for enhancing the catalytic performance of $Cu–SiO_2$ catalysts for the synthesis of ethylene glycol via the vapor-phase hydrogenation of dimethyl oxalate by coating the catalysts with dextrin, Journal of Catalysis. 350: 122–132.

[37] I. Lezcano-Gonzalez, U. Deka, B. Arstad, A. Van Yperen-De Deyne, K. Hemelsoet, M. Waroquier, V. Van Speybroeck, B.M. Weckhuysen, A.M. Beale. 2014. Determining the

storage, availability and reactivity of NH_3 within Cu-Chabazite-based Ammonia Selective Catalytic Reduction systems, Phys. Chem. Chem. Phys. 16: 1639–1650.

[38] A. Izadbakhsh, F. Farhadi, F. Khorasheh, S. Sahebdelfar, M. Asadi, Y.Z. Feng. 2009. Effect of SAPO-34's composition on its physico-chemical properties and deactivation in MTO process, Applied Catalysis A: General. 364: 48–56.

[39] X. Kong, Y. Zhu, H. Zheng, X. Li, Y. Zhu, Y.-W. Li. 2015. Ni Nanoparticles Inlaid Nickel Phyllosilicate as a Metal–Acid Bifunctional Catalyst for Low-Temperature Hydrogenolysis Reactions, ACS Catal. 5: 5914–5920.

[40] J. Gong, H. Yue, Y. Zhao, S. Zhao, L. Zhao, J. Lv, S. Wang, X. Ma. 2012. Synthesis of Ethanol via Syngas on Cu/SiO_2 Catalysts with Balanced Cu^0 –Cu^+ Sites, J. Am. Chem. Soc. 134. 13922–13925.

[41] W. Gong, C. Chen, R. Fan, H. Zhang, G. Wang, H. Zhao. 2018. Transfer-hydrogenation of furfural and levulinic acid over supported copper catalyst, Fuel. 231: 165–171.

[42] P. Panagiotopoulou, N. Martin, D.G. Vlachos. 2015. Liquid-Phase Catalytic Transfer Hydrogenation of Furfural over Homogeneous Lewis Acid-Ru/C Catalysts, ChemSusChem. 8: 2046–2054.

[43] J. Zhang, S. Wu, B. Li, H. Zhang. 2012. Advances in the Catalytic Production of Valuable Levulinic Acid Derivatives, ChemCatChem. 4: 1230–1237.

[44] A. Seretis, P. Diamantopoulou, I. Thanou, P. Tzevelekidis, C. Fakas, P. Lilas, G. Papadogianakis. 2020. Recent Advances in Ruthenium-Catalyzed Hydrogenation Reactions of Renewable Biomass-Derived Levulinic Acid in Aqueous Media, Front. Chem. 8: 221.

[45] M.N. Gebresillase, R.Q. Raguindin, H. Kim, J.G. Seo. 2020. Supported Bimetallic Catalysts for the Solvent-Free Hydrogenation of Levulinic Acid to γ-Valerolactone: Effect of Metal Combination (Ni-Cu, Ni-Co, Cu-Co), Catalysts. 10: 1354.

[46] C.-C. Tu, Y.-J. Tsou, T.D. To, C.-H. Chen, J.-F. Lee, G.W. Huber, Y.-C. Lin. 2019. Phyllosilicate-Derived $CuNi/SiO_2$ Catalysts in the Selective Hydrogenation of Adipic Acid to 1,6-Hexanediol, ACS Sustainable Chem. Eng. 7: 17872–17881.

[47] Y. Feng, S. Long, G. Yan, B. Chen, J. Sperry, W. Xu, Y. Sun, X. Tang, X. Zeng, L. Lin. 2020. Manganese catalyzed transfer hydrogenation of biomass-derived aldehydes:

Insights to the catalytic performance and mechanism, Journal of Catalysis. 389. 157–165.

[48] Z. Gao, C. Li, Y. Shao, G. Gao, Q. Xu, H. Tian, S. Zhang, X. Hu. 2021. Sequence of Ni/SiO_2 and Cu/SiO_2 in dual catalyst bed significantly impacts coke properties in glycerol steam reforming, International Journal of Hydrogen Energy. 46: 26367–26380.

[49] D.-T. To, Y.-C. Lin. 2021. Copper Phyllosilicates-Derived Catalysts in the Production of Alcohols from Hydrogenation of Carboxylates, Carboxylic Acids, Carbonates, Formyls, and CO2: A Review, Catalysts. 11:255.

[50] B. Eren, A.R. Head. 2020. Carbon Monoxide Adsorption on Manganese Oxide/Cobalt: an Ambient Pressure X-ray Photoelectron Spectroscopy Study, J. Phys. Chem. C. 124: 3557–3563.

[51] Y.-C. Liang, C.-C. Wang. 2018. Surface crystal feature-dependent photoactivity of ZnO–ZnS composite rods *via* hydrothermal sulfidation, RSC Adv. 8: 5063–5070.

APPENDICES

APPENDIX A

CALCULATION FOR CATALYST PREPARATION

The calculation of all Phyllosilicate catalysts prepared by ammonia evaporation hydrothermal method.

Calculation the 40% colloidal silica solution for silica 6 g

$$\text{Volume of colloidal silica} = \frac{\text{7.5 g of colloidal silica}}{\text{1.3 g/mL(density)}} = 5.77 \text{ mL}$$

Calculation the weight of 10% copper loading of phyllosilicate

$$\%\ \text{metal loading} = \frac{\text{weight of metal}}{\text{weight of metal + weight of silica}}$$

For weight of metal for 10%CuPS

$$10 = \frac{\text{weight of Cu}}{\text{weight of Cu + 6}} \times 100$$

weight of Cu = 0.667 g

For weight of Cu complex for 10%CuPS (M.W. of $Cu(NO_3)_2 \cdot 3H_2O$) = 241.6 g/mol)

Cu metal 63.546 g in $Cu(NO_3)_2 \cdot 3H_2O$) = 241.6 g

$$\text{Cu metal 0.667 g in } Cu(NO_3)_2 \cdot 3H_2O) = \frac{0.667 \times 241.6}{63.546} = 2.536 \text{ g}$$

Calculation of 30% wt. ammonia solution (metal: NH3 = 1:12) by mol for 10%CuPS

$$\text{Mol Cu} = \frac{0.667 \text{ g of Cu}}{63.546 \text{ g/mol}} = 0.0105 \text{ mol Cu} \times 12 = 0.1260 \text{ mol } NH_3$$

$$\text{Mol } NH_3 = 0.1260 \text{ mol } NH_3 \times \frac{17 \text{ g}}{1 \text{ mol}} \times \frac{100 \text{ g}}{30 \text{g}} \times \frac{1 \text{ml}}{0.9 \text{ g}} = 7.84 \text{ ml}$$

Table A1 the summary of CuPS

Catalyst	$Cu(NO_3)_2 \cdot 3H_2O$) (g)	Colloidal silica solution (mL)	Ammonia solution (mL)
10%CuPS	2.5360	5.77	7.85
20%CuPS	5.7030	5.77	12.64
30%CuPS	15.2078	5.77	47.60

APPENDIX B

CATALYST CHARACTERIZATION

1. X-ray Photoelectron Spectroscopy (XPS)

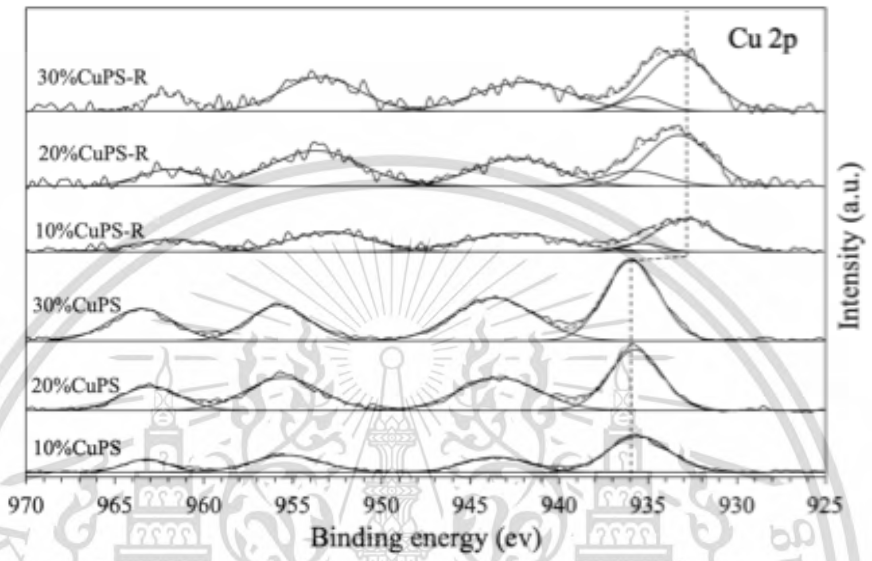

Figure B1 XPS spectra of Cu 2p of CuPS catalysts after calcination and reduction CuPS catalysts

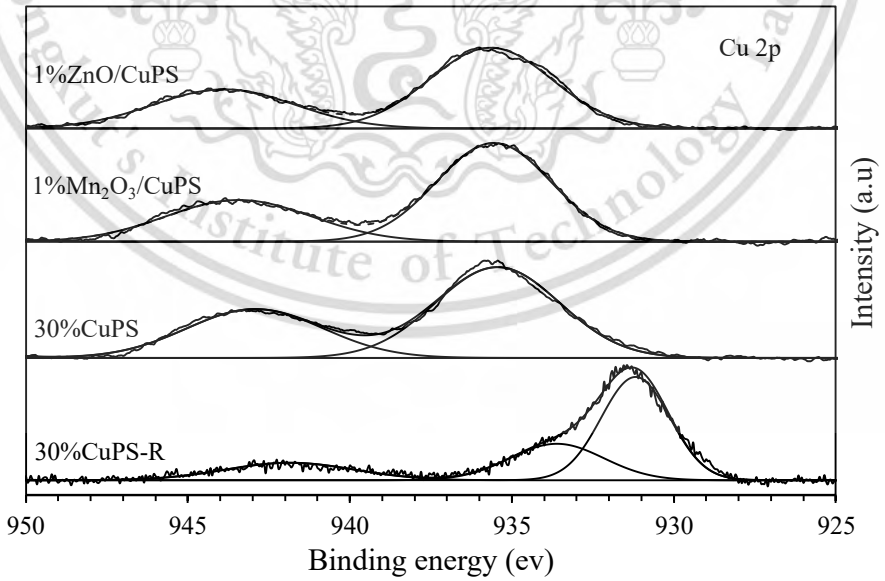

Figure B2 XPS spectra of Cu 2p of secondary metal over CuPS catalysts.

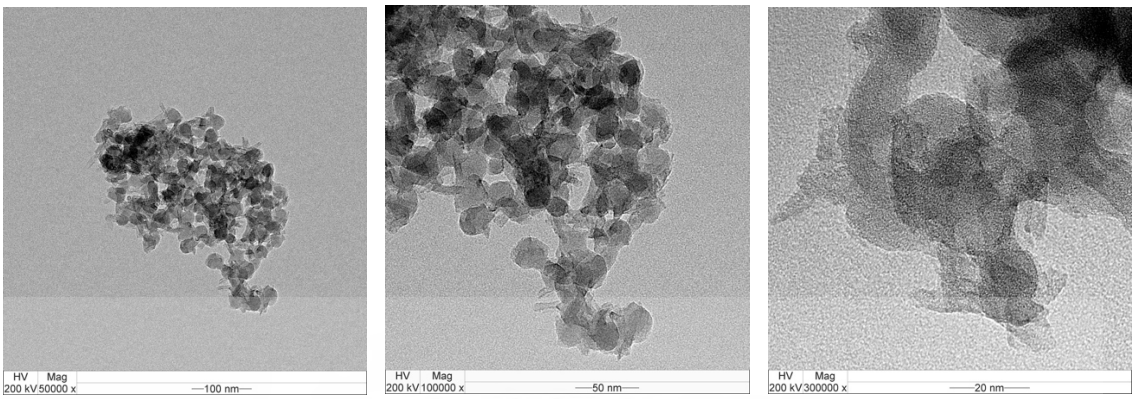

Figure B3 TEM of 10%CuPS

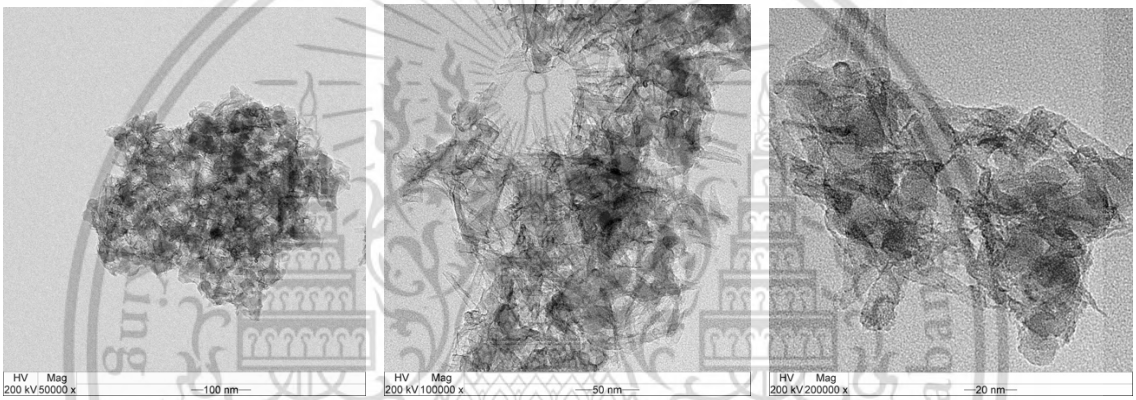

Figure B4 TEM of 20%CuPS

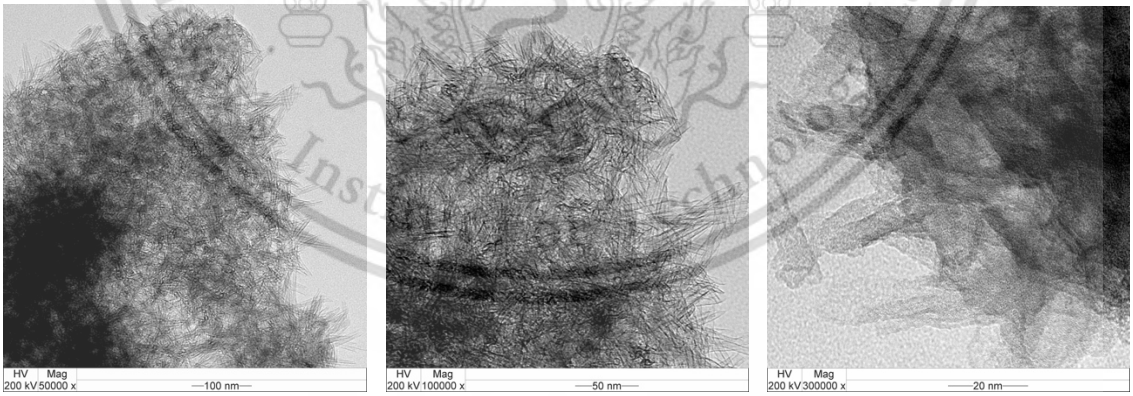

Figure B5 TEM of 30%CuPS

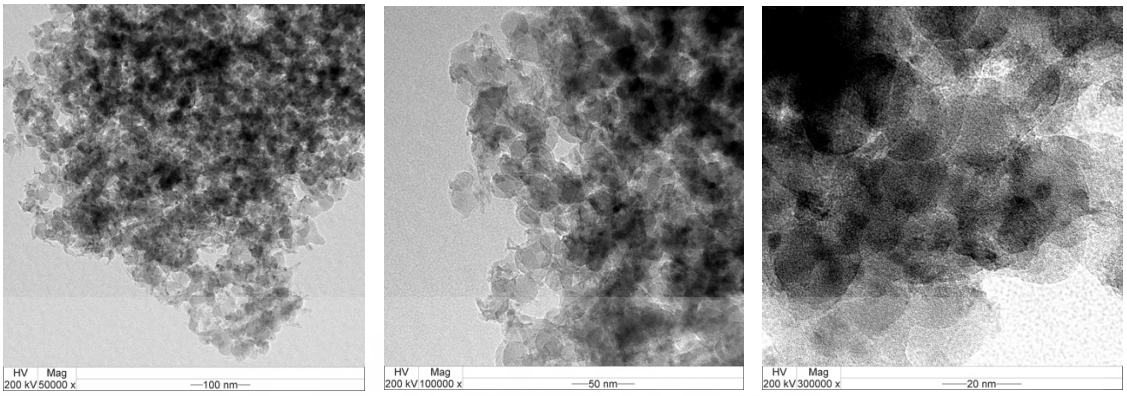

Figure B6 TEM of 10%CuPS-R

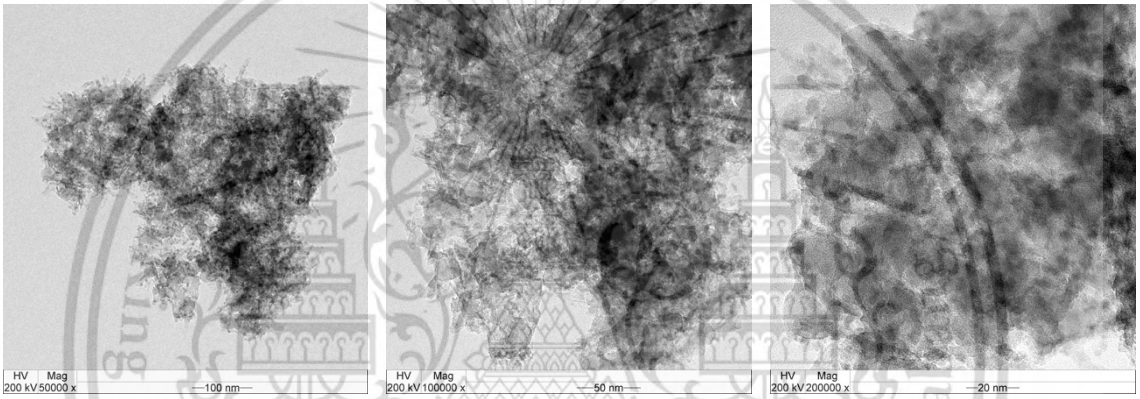

Figure B7 TEM of 20%CuPS-R

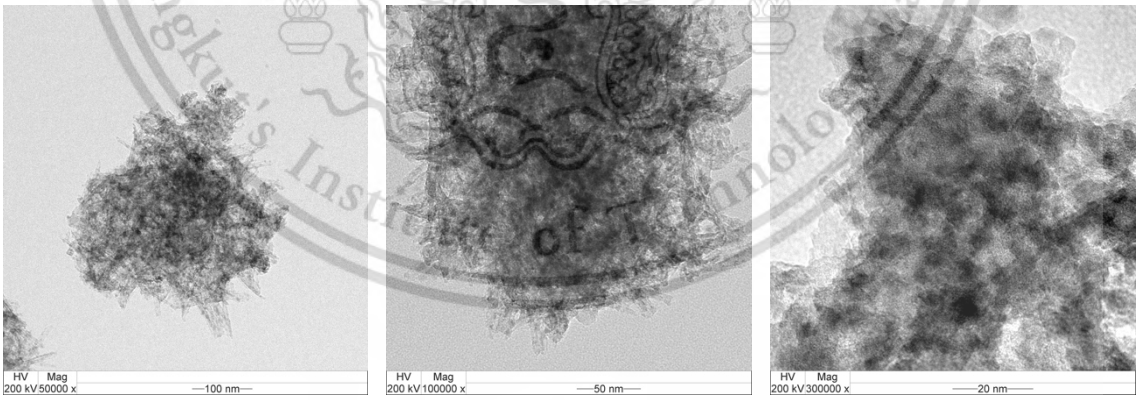

Figure B7 TEM of 30%CuPS-R

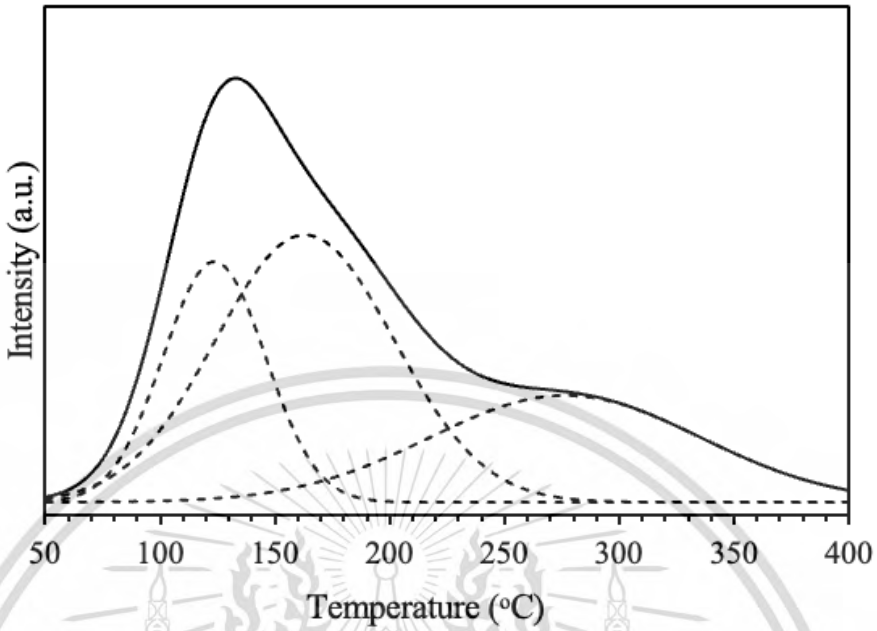

Figure B8 NH_3-TPD of 10%CuPS-R

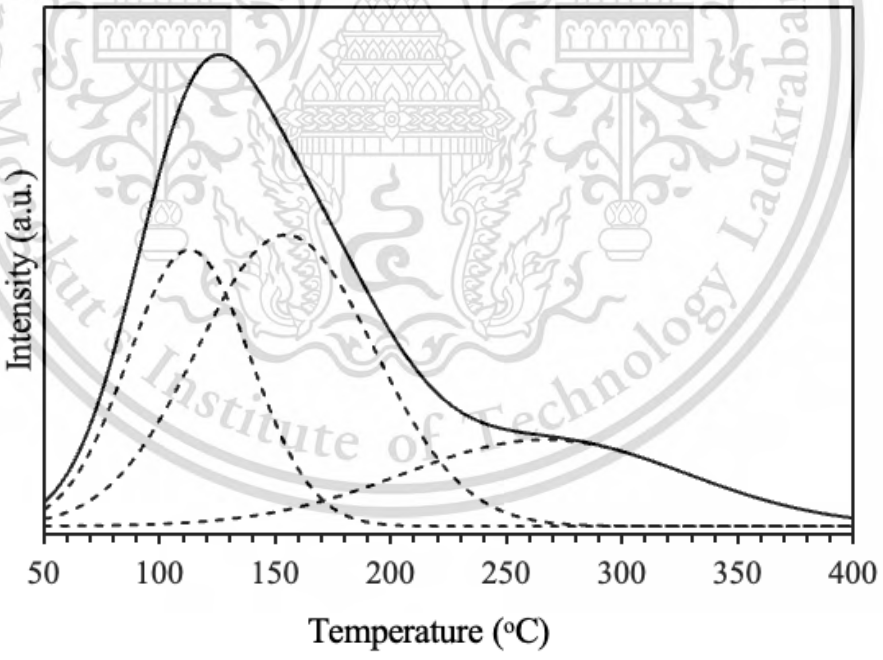

Figure B9 NH_3-TPD of 20%CuPS-R

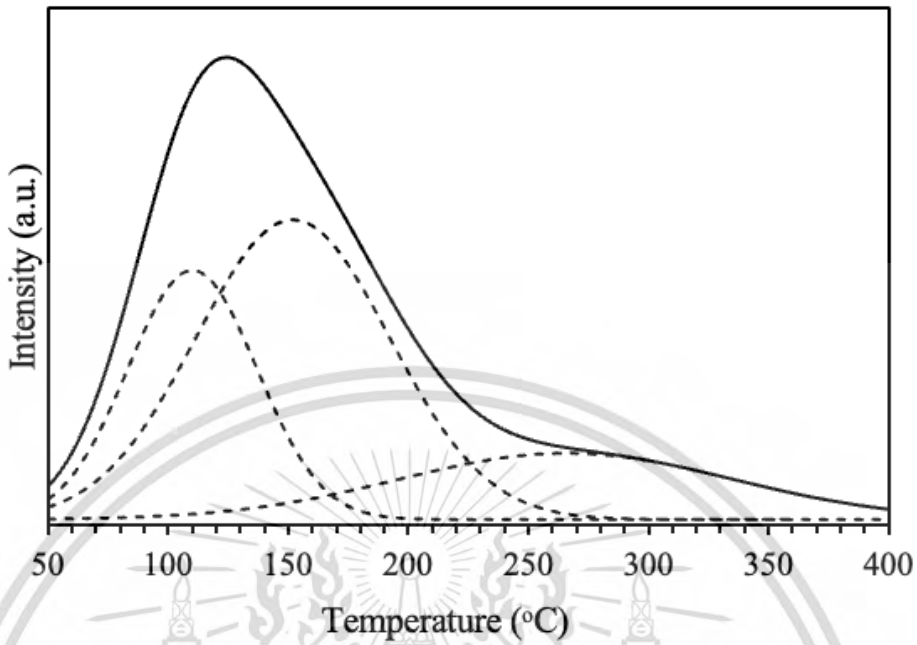

Figure B10 NH_3-TPD of 30%CuPS-R

APPENDIX C

REACTION DATA

TPR SIGNAL EVALUATION

The electronic signal from the TCD detector during TPR analysis is converted to mmol H_2, employing CuO as a standard. Here, CuO is used because it is a highly- reducible metal with clean and well-known reduction giving Cu metal as a final product following the equation:

$$CuO(s) + H_2(g) \longrightarrow Cu(s) + H_2O(g)$$

Acidity

NH_3-TPD

$$\text{Calibration value (CV)} = \frac{(\text{loop volume x \% analytical gas})}{\text{calibration area}}$$

Volume (μL) = CV x analytical area

$$\text{Amount adsorbed (μmol)} = \frac{\text{Pressure(atm) x V (μL)}}{\text{R (L x atm/K/mol) x (loop temperature (°C)+ 273.15)}}$$

$$\text{Uptake (μmol/g)} = \frac{\text{Amount adsorbed (μmol)}}{\text{Catalyst weight (g)}}$$

GC-CHROMATOGRAM

Prior to analysis, the products were identified by standard sample. Then, quantitative analysis was carried out with GC-FID (Gas chromatography equipped with Flame Ionization Detector). The analytical conditions of products from catalytic transfer hydrogenation of furfural to GVL are shown in Table C1 and Table C2 respectively.

Table C1 GC conditions for from catalytic transfer hydrogenation of furfural to GVL

column	Rtx-5
Temperature program	45 °C to 260 °C
Carrier gas	Nitrogen gas
Injection	260 °C
Detector	FID (260 °C)
Internal standard	10%Toluene/methanol

Table C1 Product distribution of physical mixing (50:50) from the measurement by GC-FID[a]

product	area	Response factor
FA	10479.1	1.15
GVL	83675.7	1.19
FE	15127.0	1.10
IPL	19860.1	1.20
LA	11590.5	0.98

[a] reaction condition: reaction conditions: furfural 200 µL (2.4 mmol), Isopropanol 10 mL, N_2 10 bar ,160°C, 2h.

Calculation of furfural conversion, GVL selectivity and reaction yield

Calculation of conversion

Conversion can be calculated from the following equation:

Corrected area is a mathematic term where the area of interested is divided by the area of the standard. A

$$\text{Corrected area of A} = \text{Area of } \frac{\text{A}}{\text{Internal standard}}$$

$$\text{Conversion (\%)} = \frac{(\text{Corrected area of initial feed} - \text{Corrected of feed at any time})}{\text{Corrected area of initial feed}} \times 100$$

For example, Physical mixing (50:50)

FF Conversion (%) of physical mixing (50:50)

$$\text{FF Conversion (\%)} = \frac{(0.41) - (0.0)}{(0.41)} \times 100 = 100\ \%$$

Calculation of Yield

Calculate the percent yield of each component in sample as follow:

$$\text{\% Yield in each product} = \frac{(\text{Corrected area of product/ Response factor})}{(\text{Corrected area of FF/ Response factor})} \times 100$$

For example, Physical mixing (50:50)

GVL yield (%) of physical mixing (50:50)

$$\text{\% Yield of GVL} = \frac{(0.27/1.19)}{(0.41/1)} \times 100 = 56.2\ \%$$

Calculation of selectivity

% Selectivity can be obtained from the following equation:

$$\% \text{ Selectivity in each product} = \frac{\text{Corrected area of product/ Response factor}}{\text{Total corrected area of product}} \times 100$$

For example; Physical mixing (50:50)

GVL selectivity (%) of **Physical mixing (50:50)**

$$\% \text{ Selectivity of GVL} = \frac{0.27}{(0.27 + 0.049 + 0.065 + 0.04)} \times 100 = 56.1\ \%$$

The catalytic activity of all catalysts.

Table C2 The catalytic performance of CuPS after calcination at 400 °C

Catalyst	Conversion (%)	Yield (%)				Selectivity (%)			
		FA	GVL	IPL	LA	FA	GVL	IPL	LA
10%CuPS	6.6	0	1.1	5.5	0	0	16.6	83.4	0
20%CuPS	15.6	0	4.0	11.6	0	0	25.6	74.4	0
30%CuPS	13.5	0	5.0	5.6	2.9	0	37.0	41.5	21.5

reaction condition: reaction conditions: furfural 200 µL (2.4 mmol), Isopropanol 10 mL, N_2 10 bar ,160°C, 2h.

Table C3 The catalytic performance of CuPS after reduction at 250 °C

Catalyst	Conversion (%)	Yield (%)				Selectivity (%)			
		FA	GVL	IPL	LA	FA	GVL	IPL	LA
10%CuPS-R	24.1	20.1	0.5	0.7	2.8	83.7	2.0	2.3	12.0
20%CuPS-R	100.0	88.3	18.0	0	0	89.2	18.1	0.0	0
30%CuPS-R	100.0	74.4	22.2	0	3.4	74.4	22.2	0	3.4

reaction condition: reaction conditions: furfural 200 µL (2.4 mmol), Isopropanol 10 mL, N_2 10 bar ,160°C, 2h.

Table C4 The catalytic performance of furfuryl alcohol as substrate.

catalyst	Conversion (%)	Yield (%)				Selectivity (%)			
		FF	GVL	IPL	FE	FF	GVL	IPL	FE
calcined	98.8	1.9	53.8	34.2	8.9	1.9	53.8	34.2	8.9
reduced	31.8	0.0	18.9	0.0	12.8	0.0	59.4	0.0	40.6

reaction conditions: furfuryl alcohol 200 µL (2.4 mmol), Isopropanol 10 mL, N_2 10 bar ,160°C, 2h.

Table C3 The catalytic performance of physical mixing between 30%CuPS-R and 30%CuPS catalysts with various % wt. ratios.

Catalyst	Conversion (%)	Yield (%)					Selectivity (%)				
		FA	GVL	IPL	LA	FE	FA	GVL	IPL	LA	FE
30%(Re): 70%(cal)	47.8	1.7	18.7	21.5	5.6	0	3.5	39.0	44.9	12.5	0.0
50%(Re): 50%(cal)	100.0	7.6	56.2	15.5	0	20.9	7.6	56.2	15.5	0.0	20.9
70%(Re): 30%(cal)	100.0	50.0	42.9	0.0	0.0	7.1	50.0	42.9	0.0	0.0	7.1

reaction condition: reaction conditions: furfural 200 µL (2.4 mmol), Isopropanol 10 mL, N_2 10 bar ,160°C, 2h.

Table C4 The catalytic performance of secondary metal over CuPS catalysts.

Catalyst	Conversion (%)	Yield (%)				Selectivity (%)			
		FA	GVL	IPL	LA	FA	GVL	IPL	LA
30CuPS-R	100.0	74.4	22.2	3.4	0.0	74.4	22.2	3.4	0.0
1%ZnO/30CuPS-R	61.3	55.5	5.3	0.0	0.0	90.6	8.67	0.0	0.0
1%Mn/30%CuPS-R	96.6	93.8	2.8	0.0	0.0	97.1	2.9	0.0	0.0
30CuPS-R +1%Zn/30CuPS	99.0	91.9	7.4	0.0	0.0	92.8	7.4	0.0	0.0
30CuPS-R+1%Mn/30%CuPS	100.0	95.9	4.1	0.0	0.0	95.9	4.1	0.0	0.0

reaction condition: reaction conditions: furfural 200 µL (2.4 mmol), Isopropanol 10 mL, N_2 10 bar ,160°C, 2h.

AURTHER BIOGRAPHY

Name Miss Tanyarat Shoosri

Date of Birth 11 November 1997

Address 112, 7 Sa Si Liam Subdistrict, Phanat Nikhom District, Chon Buri Province 20140

Education (2019) Bachelor of Science in industrial chemistry GPA 3.46

International Conferences

Tanyarat Shoosri, Sanchai Kuboon, Tawan Sooknoi and Patcharaporn Weerachawanasak, *"The effect of metal oxide promotors (Mn_2O_3, ZnO) on copper phyllosilicate catalysts for catalytic transfer hydrogenation of furfural to furfuryl alcohol"* , PACCON 2022, KMITL Convention Hall, King Mongkut's Institute of Technology Ladkrabang, Bangkok, Thailand.